CVR-2019-0967

Toward standardization of echocardiography for the evaluation of left ventricular function in adult rodents: a position paper of the ESC Working Group on Myocardial Function

Serena Zacchigna[1,2*], Alessia Paldino[1*], Inês Falcão-Pires[3*], Evangelos P. Daskalopoulos[4], Matteo Dal Ferro[1], Simone Vodret[2], Pierluigi Lesizza[1], Antonio Cannatà[1], Daniela Miranda-Silva[3], André P. Lourenço[3], Bruno Pinamonti[1], Gianfranco Sinagra[1], Florian Weinberger[5], Thomas Eschenhagen[5], Lucie Carrier[5], Izhak Kehat[6], Carlo G. Tocchetti[7,8], Michele Russo[7,9], Alessandra Ghigo[9], James Cimino[9], Emilio Hirsch[9], Dana Dawson[10], Michele Ciccarelli[11], Marco Oliveti[11], Wolfgang A. Linke[12], Ilona Cuijpers[13, 14], Stephane Heymans[13,14], Nazha Hamdani[15], Martine de Boer[16], Dirk Duncker[16], Diederik Kuster[17], Jolanda van der Velden[17], Christophe Beauloye[4,18], Luc Bertrand[4], Manuel Mayr[19], Mauro Giacca[1,2,19], Florian Leuschner[20], Johannes Backs[20], Thomas Thum[21] on behalf of the Working Group on Myocardial Function of the European Society of Cardiology.

[1] Department of Medicine, Surgery and Health Sciences and Cardiovascular Department, Centre for Translational Cardiology, Azienda Sanitaria Universitaria Integrata Trieste, Italy
[2] International Center for Genetic Engineering and Biotechnology (ICGEB), Trieste, Italy
[3] Cardiovascular Research and Development Center, Faculty of Medicine of the University of Porto, Porto, Portugal
[4] IREC Institute, Pole of Cardiovascular Research, Université catholique de Louvain, Belgium, Brussels
[5] Institute of Experimental Pharmacology and Toxicology, University Medical Center Hamburg Eppendorf, Germany and DZHK (German Centre for Cardiovascular Research), partner site Hamburg/Kiel/Lübeck
[6] Dept. of Physiology, biophysics and system biology, The Ruth and Bruce Rappaport Faculty of Medicine, Technion – Israel Institute of Technology
[7] Department of Translational Medical Sciences, Federico II University, Naples, Italy
[8] Interdepartmental Center of Clinical and Translational Research (CIRCET), Federico II University, Naples, Italy
[9] Department of Molecular Biotechnology and Health Sciences, Molecular Biotechnology Center, University of Torino, Torino, Italy
[10] School of Medicine and Dentistry, University of Aberdeen, United Kingdom
[11] University of Salerno, Salerno, Italy
[12] Institute of Physiology 2, University of Muenster, Germany
[13] Maastricht University Medical Centre, Maastricht University, The Netherlands
[14] Center of Molecular and Vascular Biology (CMVB), KU Leuven, Leuven, Belgium
[15] Department of Molecular and experimental Cardiology, Division Cardiology, St. Josef-Hospital, Ruhr University Bochum, and Institute of Physiology, Ruhr University Bochum, Bochum, Germany.
[16] Division of Experimental Cardiology, Department of Cardiology, Thoraxcenter, Erasmus MC, University Medical Center Rotterdam, Rotterdam, The Netherlands
[17] Department of Physiology, Amsterdam UMC, Vrije Universiteit, Amsterdam Cardiovascular Sciences Institute, Amsterdam, The Netherlands
[18] Division of Cardiology, Cliniques Universitaires Saint-Luc, Brussels, Belgium
[19] King's College London, British Heart Foundation Centre of Research Excellence, School of Cardiovascular Medicine & Sciences, London UK
[20] Department of Cardiology, Angiology & Pulmology, Heidelberg University Hospital, Germany
[21] Institute for Molecular and Translational Therapeutic Strategies (IMTTS), Hannover Medical School, Hannover, Germany

[*] These authors contributed equally to this work.

Address for correspondence:
Serena Zacchigna, MD, PhD
Cardiovascular Biology Laboratory, ICGEB and University of Trieste, Italy
Padriciano, 99, 34149 Trieste, Italy
Tel. +39 040 3757 354/214/357, Fax +39 040 226555
e-mail: zacchign@icgeb.org
www.icgeb.org/group-leader-serena-zacchigna.html

ABSTRACT

Echocardiography is a reliable and reproducible method to assess non-invasively cardiac function in clinical and experimental research. Significant progress in the development of echocardiographic equipment and transducers has led to the successful translation of this methodology from humans to rodents, allowing for the scoring of disease severity and progression, testing of new drugs, and monitoring cardiac function in genetically modified or pharmacologically treated animals. However, as yet, there is no standardization in the procedure to acquire echocardiographic measurements in small animals. This position paper focuses on the appropriate acquisition and analysis of echocardiographic parameters in adult mice and rats, and provides reference values, representative images and videos for the accurate and reproducible quantification of left ventricular function in healthy and pathological conditions.

Introduction

Monitoring the function of the left ventricle (LV) is a key element in experimental studies aimed at understanding the pathophysiology of cardiac diseases and in exploring the beneficial effect of innovative therapies. Echocardiography is often the technique of choice to evaluate cardiac function in rodents, with the advantage that it is non-invasive, safe, reproducible, widely available, and inexpensive. The efficacy of new therapeutics in small animal models is key for their further application in larger animal models and humans [1, 2]. However, only a small percentage of the therapeutics showing efficacy in small animals actually progresses to clinical use [3, 4]. One of the possible reasons for this lack of translatability is the nonexistence of standards and minimal requisites to ensure reliable and accurate evaluation of cardiac function in rodents. A detailed description and standardization of the methods used for data acquisition and analysis would add further value to studies performed by expert groups [5-8]. While some suggestions and recommendations have appeared in the literature in recent years [9-12], we believe it is crucial define the conditions to standardize the evaluation of LV function in small rodents using echocardiography. Standardized and well-defined echocardiographic conditions will aid both authors and reviewers in evaluating the accuracy of cardiac function data derived from small rodents.

This paper also includes reference values for adult mice and rats (**Tables 1** and **2**), echocardiographic routines for assessing specific pathologic conditions (**Table 3**), common pitfalls to avoid in the echocardiography of rodents, and reference to scientific literature for specific methodological details. Although we could not include all publications available in this expanding field, representative studies supporting our statements have been cited.

1. Minimal requirements for echocardiographic evaluation in rodents

Considerable progress in technology and equipment have made the detailed evaluation of cardiac structure and function possible in small rodents. While pioneering studies used clinical echocardiographic systems [13], modern and high-frequency instruments specifically designed for small animal hearts are now available and capable to acquire both improved high-frame-rate and near-field images [14, 15]. For echocardiography in mice, we recommend transducers with a center frequency of at least 30 MHz (body weight >35 g) or 40 MHz (body weight <35 g), with a real-time imaging frame-rate of more than 30 frames per heartbeat [16]. For advanced image analysis, such as speckle tracking or myocardial strain, frame-rates of 100 frames per heartbeat are recommended in mice [17]. For Doppler studies, the ultrasound (US) probe should be capable of recording a peak velocity higher than 1500 mm/s in mice. Currently, echocardiographic images in rats can be obtained using conventional frequencies in the 10-15 MHz range [18]. However, advances in dedicated small animal echocardiography can lead to improved image quality using higher frequencies.

Additional equipment is essential for the echocardiographic exam, i.e. electrocardiography (ECG) electrodes connected to the US machine, a temperature probe. and either a heating pad or a heat lamp source, to maintain the animal's physiological body temperature. Furthermore, a vaporizer is required to administer volatile anesthetics, and limited ambient light during the acquisition is recommended to obtain optimal contrast.

2. Preparation of the animal

2.1. Anesthesia

A few studies encourage performing echocardiography in conscious rodents after acclimatizing them to the researcher and the environment[19]. However, unlike humans and large animals, echocardiography without anesthesia is highly stressful for rodents, leading to variations in stress response between groups that might mask pathology-induced differences, particularly in diastolic function assessment. In addition, working with conscious animals can often also be very stressful for the researchers. Thus, we recommend anesthetizing the animals to increase the reproducibility of the measurements and to reliably compare data obtained between groups [11, 20]. However, it should be taken into consideration that the induction of the anesthesia might vary significantly with age, strain, liver/lung function, obesity, and other diseases such as heart failure (HF), sepsis, etc. For instance, special attention should be given to models of ischemia/reperfusion, wherein some anesthetics, such as halogenated gases and opioids, have been shown to interfere with cardioprotection [21, 22]. **Supplementary Table 1** provides reference values for conscious mice, to be adopted if the experimental conditions require avoiding the use of any type of anesthesia.

Most anesthetics have negative inotropic and chronotropic effects. For instance, tribromoethanol (e.g. Avertin™), pentobarbital (e.g. Eutha 77™) and ketamine (e.g. Ketaset™) have all shown to depress cardiac function. The most popular anesthetics are either a mixture of ketamine/xylazine (e.g. Rompun™; 100/10 mg/kg i.p., respectively) or halogenated gases, such as isoflurane (1-2%)[11, 18, 23] and sevoflurane (3-4%) [24]. These gases should be delivered in 21% oxygen and 79% nitrogen mixture [25, 26], although an oxygen-enriched gas mixture is widely used and accepted. While ketamine is the only anesthetic that increases blood pressure and heart rate (HR) [27], its combination with xylazine results in cardio-depression. On the contrary, halogenated gases are now preferred, due to their easy titration, fast reversibility and, most importantly, minimal cardiovascular depression. For a more detailed overview of the advantages and limitations of the most common anesthetics used during echocardiography in mice, see Lindsey et al. [9, 10]. In rats, ketamine/xylazine and isoflurane are among the most commonly used anesthetics during echocardiographic acquisition. Their comparison has been essentially performed in healthy rats, in which cardio-depressive effects, without changes in systolic and LV dimension indexes, were induced by ketamine/xylazine but not by isoflurane [28-30]. Although useful, the uptake and/or effect of anesthetics in diseased rats might differ. While further research is required to precisely determine the effects of different anesthetics on hemodynamic, systolic, LV dimension, and diastolic indexes in both mice and rats, this position paper suggests the use of halogenate gases as the first-line choice for rodent echocardiography.

2.2. Monitoring physiological parameters

Cardiac function depends on multiple physiological parameters, including HR, body temperature, respiratory rate, blood pressure and oxygenation levels, which are all influenced by most anesthetics. Although the instrumentation and expertise to accurately monitor blood pressure and oxygenation levels in rodents is not available in most laboratories, body temperature, HR and respiratory rate can be easily monitored during rodent echocardiography. While blood pressure and oxygenation levels provide a direct measure of potential anesthetic cardio-depressant actions, body temperature, HR, and respiratory rate provide an indirect estimate of the impact that changes in the autonomic nervous system might impose during the exam. Body temperature can be measured using a rectal probe, and maintained within its physiological range (35.5 – 37.5°C) using a dedicated heating pad. Anesthetized animals are unable to control and maintain their physiological body temperature, which is a major determinant of several cardiovascular function indexes. Rats, in particular, are at higher risk for hypothermia due to their high body surface to body mass ratio. In addition to anesthesia, the resting-state, shaving, and application of echocardiography gel further increase the risk of hypothermia. As such, continuous monitoring of body temperature by a rectal probe is recommended to regulate the heating and maintain the body temperature.

HR can be monitored by ECG, either by taping electrodes to the paws or laying the animal on a platform equipped with electrodes. When monitoring the HR, differences between strains [31-33] and specific experimental conditions can have a major impact and should be considered when performing echocardiography. When starting the measurements, the transducer should be covered by warm gel and applied gently to avoid chest compression, thereby minimizing cardiovascular reflexes, such as bradycardia and hypotension. For the most commonly used rodent models, any intervention/anesthesia lowering the HR to values below 450 beats per minute (bpm) in mice and 350 bpm in rats is considered to exert cardio-depression, i.e. concomitant negative inotropic and chronotropic effects. This compromises the reliability of cardiac parameters assessed, as shown in Table 2, in which reference values are split in separate columns for mice kept at a physiological HR (≥ 450 bm) or depressed by anesthesia (HR < 450 bpm). While we believe that this threshold should be applied to most studies to ensure the contextual evaluation of both systolic and diastolic function (see also below), a lower HR could be acceptable in experimental settings that result in decreased basal HR, e.g. in the presence of a beta-blocker. However, in such studies, authors should provide an explanation as to why HR is low. In any case, consistency of HR values between experimental groups has to be demonstrated and HR values should always be reported together with the functional measurements.

A description on how to start and finalize the echocardiographic exam is depicted in **Figure 1**.

3. Echocardiographic techniques

Similar to humans, echocardiography imaging in rodents can incorporate five main modalities, in several views and planes: i) motion mode (M-mode), ii) two-dimensional (2D) brightness mode (B-mode), iii), Doppler imaging, iv) speckle tracking echocardiography (STE), and v) three/four-dimensional (3D/4D) imaging.

3.1. M-mode

The M-mode can be used for the assessment of systolic function and LV size. M-mode tracing can be performed in either the parasternal long- or short-axis (**Figure 2**). To obtain a parasternal long-axis of the heart, the animal is laid in a supine position and the US transducer should be placed on the left side of the animal's chest, with the notch pointed toward its right shoulder. The following features should be considered as indicators of an appropriate long-axis view: i) the aortic valve, the proximal course of aortic root and ascending aorta and the left ventricle apex are visible; ii) the LV is positioned in the center of the field of view; iii) the base-to-apex axis is parallel to the transducer surface, corresponding to the longest axis (**Figures 2** and **3**). Usually, the right ventricle (RV) can be partially seen in this view. From this position, a 90° rotation of the transducer clockwise generates the short-axis images. From this view, M-mode tracings are optimally acquired at the level of the papillary muscles, which should be simultaneously visible in the antero-lateral and postero-medial quadrants of the heart, respectively [34]. In the short-axis view, the LV should have a round shape, which should be maintained while moving through the long-axis of the LV from base to apex (**Figures 2** and **3**). If it appears oval, the LV is most likely being imaged obliquely. Common pitfalls include, but are not limited to, off-axis views, inclusion of RV trabeculae as part of the septum, and acquiring a short-axis recording at the papillary muscle rather than the posterior wall (**Figure 3**).

3.2. B-mode

The B-mode can be applied to all echocardiographic views. Together with a four-chamber view, the parasternal long-axis view can be used in rodents for studying LV volumes and function. While in humans the LV apex is not included in parasternal long-axis view and is commonly visualized in either the four- or the two-chamber view, the larger size of the transducer, relative to the size of the heart, permits good visualization of the apex together with basal and medium segments of the anteroseptal and posterior LV wall in rodents (**Figure 2**). Particular attention should be taken to avoid foreshortened or truncated views with a ‘false’ apex, as could be suggested by a spherical, not elliptical, shape of the LV (**Figure 3**). Based on the parasternal long-axis view, as described in Section 3.1, LV images are extracted from the cine-loop recordings at the end of both systole and diastole. These specific time points are recognized as optimal if the ECG is simultaneously recorded and displayed [35]. Here, the end of the diastole corresponds to the frame in which the LV reaches its maximal extension (LVEDA, LV end-diastolic area), whereas the end of systole corresponds to the minimal size of the LV area (LVESA, LV end-systolic area).

B-mode imaging is also frequently used for multiplane evaluations for several purposes, such as assessment of valve function, cardiac output, vessel size, and more accurately measured LV volumes (using a modified Simpson’s rule as described below[36]). This approach combines the measurements taken from multiple views, including the parasternal long-axis and at least three short-axes i) at the level of the base, ii) at an intermediate position, approximately at the level of the papillary muscles, and iii) at the apex level (**Figures 2** and **4**).

3.3. Doppler analysis

Pulsed-wave (PW) Doppler is used to assess the myocardial and flow-velocity profiles of moving objects or structures, which are particularly useful in assessing diastolic function. It is based on the Doppler principle, by which wave frequencies change every time they are reflected by moving targets. For instance, when the reflected waves are moving toward the receiver, each successive wave is reflected from a position closer to the receiver than the previous one. Hence, the time between the arrivals of successive waves at the observer is reduced, causing an increase in their frequency. Conversely, if the target is moving away from the receiver, each wave is reflected from a position farther from the receiver than the previous one, so the arrival time between successive waves is increased, reducing the frequency. This is why any change in blood flow velocity can be appreciated as a Doppler shift [10, 24].

In humans, Doppler shift can be assessed either continuously, when two separated transducers simultaneously emit and receive Doppler signals, or pulsed, when the same transducer alternatively emits and receive the signals in a pre-specified volumetric region or scan line. Color Doppler indicates the mean velocity in discrete ranges, which are displayed in different colors. Any movement away from the transducer is generally indicated in blue and movements towards the transducer are indicated in red. In rodents, PW and color Doppler are commonly used to display the velocity of moving objects inside the heart and blood vessels. In the case of PW and color Doppler, the moving objects are blood cells, while in tissue Doppler Imaging (TDI), the moving target is the myocardial tissue. In both cases, the user has to select the targeted sample blood/myocardial volume by placing the sample volume over this area, and to ensure that the Doppler beam is aligned with the direction of the moving objects to avoid underestimation of their velocity [10, 24]. Special attention should be given to the position of the sample volume, as missing the highest velocities seems to be one of the most common pitfalls in assessing diastolic function in rodents (**Figure 3**).

Compared to blood, the velocities of the moving tissue are much lower and the amplitude of the backscattered signal from tissue is much larger, therefore the velocity scale must be reduced to values near the 30-60 mm/s and the gain minimized. Myocardial movement analysis by TDI presents some limitations, in that myocardial structures are constantly moving longitudinally and circumferentially, and passive motion is difficult to separate from active movement.

Usually, PW and TDI analysis are performed at the four-chamber view, which can be obtained by placing the transducer over the apex and pointing it medially towards the animal's head, so that the beam crosses both ventricles, both atria, and their respective walls and septa. This view enables both a good orientation of a Doppler mitral and tricuspid flow signal and the acquisition of tissue Doppler signals near the mitral and tricuspid valve annuli [24]. Again, placing the sample volume in the optimal position guarantees the acquisition of maximal velocities.

3.4. Speckle Tracking Echocardiography

Modern small animal instrumentation allows the visualization of myocardial deformations by speckle tracking echocardiography (STE) and quantitative evaluation of both global and regional myocardial function, independently from both insonation angle and cardiac translational movements [37]. As in humans, accurate STE acquisition in animal models requires images with a clear visualization of both endocardial and epicardial borders and a high frame rate (at least 100 frames per heartbeat) [17].

Several tracking points should be placed on the endocardial border to semi-automatically trace the endocardial and epicardial border, in both long and short-axis views at the level of the papillary muscles. Both axes are automatically divided in multiple segments for the quantification of: i) displacement, which defines the distance that each point has moved between two consecutive frames, ii) velocity, which reflects displacement per unit of time, iii) strain, which reflects the deformation of an object normalized to its original shape and size, and iv) strain rate, which describes the rate of strain or in other words how fast the deformation occurs. Strain and strain rate are preferable to velocity and displacement data, as the recording of velocity and displacement is influenced by movements of the chest during breathing, while strain and strain rate are not. These parameters allow the discrimination of myocardial active and passive movements, and the separate assessment of distinct components of myocardial deformation, such as lengthening, shortening, thickening, twisting and torsion [38]. Thus, more complex geometric aspects are implicated in the estimation of LV contractility by STE compared to standard echocardiography [39]. Values of strain and strain rate can be obtained for the longitudinal, radial, and circumferential axes, both globally and in each segment.

In humans, global longitudinal strain, obtained as the average of the longitudinal strain of each myocardial segment recorded from the three apical views, is the most accepted and studied STE-derived parameter of systolic function [40]. Due to its ability to detect and quantify local impairments in cardiac contractility, STE is widely used in the clinics, particularly to detect subclinical stages of myocardial dysfunction in a broad range of pathologies that have not yet resulted in increased volumes or compromised EF. These include: i) the detection of small, recent and sub-endocardial myocardial infarction [17, 41-45] , ii) the detection of subtle systolic dysfunction in patients with heart failure with preserved ejection fraction (HFpEF) [46-48], iii) the discrimination between physiological and pathological LV hypertrophy [49], iv) the early diagnosis of chemotherapy-induced cardiac toxicity [50-53], and v) the identification of sub-clinical cardiac dysfunction in relatives of patients affected by genetic forms of dilated cardiomyopathy [54, 55].

While STE is becoming more widely used, most of the rodent studies published in high-impact journals of general interest do not include strain analysis [56-66]. Since all US-based images have better resolution if acquired along the US beam, STE is not completely angle-independent [67] and values obtained in the parasternal long-axis view in rodents may be less accurate compared to those in humans. An additional, current limitation is the absence of reference values, the definition of which will require more widespread use of this technology in animal models to ensure reproducibility and accuracy. Examples of STE in healthy, hypertrophied and infarcted hearts are depicted in **Videos 1-6**.

3.5. Three/four-dimensional (3D/4D) imaging

Modern instrumentation for both human and small animal echocardiography allows the 3D volumetric reconstruction of cardiac chambers. The software analyzes LV geometry (volume and mass) upon the acquisition of multiple serial images at a pre-defined distance (micrometric slices), using a motor that moves the transducer along the long-axis. These slices can be eventually merged and combined with a temporal dimension (4D) through automated respiratory and ECG gating. Volumes at late systolic and diastolic time points are acquired as post-processing analysis.

Theoretically, 3D/4D imaging appears as the most reliable method for assessment of cardiac chamber volume and function, being based on real, imaged-based endocardial and epicardial tracing and not on geometrical assumptions. The additive value of 3D/4D imaging over B-mode single- and multi-plane methods for the evaluation of volumes and systolic function and its comparison with the gold standard magnetic resonance imaging (MRI) has been demonstrated by a few pioneering studies in rodents [68, 69]. It has also been applied to genetic models of cardiac dysfunction. However, this echocardiographic technique has several limitations, including the need for accurate ECG and respiratory gating by sophisticated equipment (often not available in standard laboratories), the generation of extensive data, requiring powerful computational resources for analysis, and moderate reproducibility [69]. While anatomic structures (i.e. ribs, sternum, lungs) could interfere with 3D heart reconstruction, the relatively low cost, rapid acquisition time, and high spatiotemporal resolution are expected to promote the use of 3D/4D echocardiography for the evaluation of LV function in small animals.

While reference values for 3D/4D-generated data on human cardiac dimensions and mechanics have recently been provided [40], large databases have not yet been built for rodents and it is therefore premature to provide reference values. 4D videos from healthy mice and well as from hearts subjected to chronic pressure overload and myocardial infarction are provided (**Videos 7-9**, respectively).

4. Evaluation of systolic function

To evaluate systolic function in rodents, three major imaging views are used: M-mode single-plane evaluation, and B-mode single- and multi-plane evaluation.

4.1. M-mode (single-plane) parasternal short-axis view

M-mode tracing on the short-axis has been the most commonly used method to measure systolic function in both mice and rats [56-66, 70, 71]. M-mode images are displayed as a continuous function of time, allowing optimal temporal resolution and precise quantification of wall thickening [72]. Measurements have to be taken in both systole and diastole, which requires simultaneous ECG recording. The start of the QRS complex on the ECG marks the end of diastole, the time point at which diastolic measurements should be acquired. Systolic measurements can be made at either the zenith of the posterior wall motion or the nadir of the anterior wall motion. These two events do not occur exactly at the same time, neither in humans nor in rodents. However, they can both be used as a reference for systolic measurements with the same level of accuracy, which results in comparable values. In the case of a large myocardial infarction, the anterior wall motion is often compromised and the use of the posterior wall peak motion is recommended.

The leading edge method, in which measurements are calculated from the side closest to the transducer towards the leading edge of the following echo, allows the quantification of the following LV parameters both in systole and diastole (**Figure 2**): anterior wall thickness (LVAWs and LVAWd), posterior wall thickness (LVPWs and LVPWd), and internal diameters (LVIDs and LVIDd) [73]. From these values, fractional shortening (FS), LV end-systolic and end-diastolic volumes (LVESV and LVEDV), and ejection fraction (EF) can be calculated, applying the following formulas [74]:

$$\text{FS (\%)} = (\text{LVIDd} - \text{LVIDs})/\text{LVIDd} \times 100$$

$$\text{LVESV} = (7/(2.4 + \text{LVIDs})) \times \text{LVIDs}^3$$

$$\text{LVEDV} = (7/(2.4 + \text{LVIDd})) \times \text{LVIDd}^3$$

$$\text{EF (\%)} = (\text{LVEDV} - \text{LVESV})/\text{LVEDV} \times 100$$

However, since M-mode tracing records cardiac contraction on a single spatial plane, these calculations rely on geometrical and mathematical assumptions that do not exactly represent the shape of the heart. In particular, the change in volume during systole and diastole derives from linear changes measured on the short-axis, without any contribution from longitudinal contraction. Moreover, the shape of the LV is assumed to be a modified ellipsoid, whereas the physiological LV often has an irregular shape, particularly after myocardial infarction, asymmetric septal hypertrophy or RV failure [36].

Furthermore, it should be taken into account that any error in the tracing significantly reduces the accuracy of the data, as the measurements are raised to the third power for the calculation of LV volumes. Finally, the accuracy of this method is further limited in case of segmental wall motion abnormalities, i.e. in the post-myocardial infarction, particularly at the apex. Therefore, B-mode evaluation is preferred to properly evaluate systolic function in most experimental models.

LV mass can be estimated using Devereux's formula [75], modified for rodents:

$$\text{LV mass} = 1.04\ [(\text{LVIDd} + \text{LVAWd} + \text{LVPWd})^3 - \text{LVIDd}^3] \times 0.8 + 0.6$$

The formula to calculate LV mass is derived from the formula applied in humans, where 1.04 is the estimated specific gravity and the remaining constants are correction factors. Importantly, the values of LV mass significantly correlate with post-mortem LV weight in normal Sprague-Dawley rats [76] and hypertensive Dahl-salt rats [77].

Another option when computing LV mass is by using the less common area-length method [78]. Although it seems more accurate, it warrants validation to determine the degree of correlation with LV weight or LV mass assessed by 3D-echocardiography. In a simplistic view, LV mass is estimated by subtracting the volume of an ellipse corresponding to the LV cavity from the total LV volume (wall + cavity). To accomplish this, one should trace the epicardium and endocardium in midventricular parasternal short-axis view, calculate the average myocardial wall thickness ((LVAWd + LVPWd) / 2), and apply the following formula:

$$\text{LV mass} = 1.05 \times [5/6 \times \text{EpiC} \times (\text{LVEDL} + (\text{LVAWd} + \text{LVPWd}) / 2)] - (5/6 \times \text{EndC} \times \text{LVEDL})$$

where EpiC, and EndC correspond to epicardial and endocardial areas in diastole, respectively, and LVEDL is the end-diastolic LV length, corresponding to the distance from the aortic annulus to the endocardial border of the apex (measured in B-mode, long axis).

4.2. B-mode (single-plane) parasternal long-axis view

Aortic diameter and left atrial (LA) area can be measured in parasternal long-axis orientation using the B-mode, although we recommend measuring LA area in the four-chamber view. Tilting the transducer slightly in this position reveals the RV and pulmonary artery, thereby allowing assessment of the total RV and RV outflow tract dimensions in M-mode, as well as the pulmonary velocity-time integral (VTI) using PW Doppler.

Using a mono-plane of the parasternal long-axis view in B-mode, a significant number of systolic indexes and volumes can be obtained. This is achieved by tracing the endocardial border around the LV cavity at the end of both systole and diastole, thereby generating the LV end-diastolic and end-systolic area (LVEDA and LVESA, respectively) and by measuring the LV length at end-diastole and end-systole, respectively (LVEDL and LVESL), as shown in **Figure 2** and according to the following formulas:

$$\text{LVEDV} = 8 \times \text{LVEDA}^2/3\ \pi\ \text{LVEDL}$$

$$\text{LVESV} = 8 \times \text{LVESA}^2/3\ \pi\ \text{LVESL}$$

Based on these calculations, other systolic function parameters can be determined [79, 80], such as stroke volume (SV, volume of blood ejected from the LV during systole), and cardiac output (CO, volume of blood ejected from the LV per minute). In the case of large differences in body weight (BW), cardiac output should be normalized to body surface area (BSA) and expressed as cardiac index (CI). Below, the corresponding formulas are given:

$$\text{SV} = \text{LVEDV} - \text{LVESV}$$

$$\text{CO} = \text{SV} \times \text{HR}$$

$$\text{CI} = \text{CO} / \text{BSA}$$

$$\text{BSA} = 9.8 \times \text{BW}^{2/3}$$

Similar to M-mode images, these calculations are also based on the geometrical assumption that the LV has a modified ellipsoid shape [36]. Again, this can generate inaccuracy, particularly when motion abnormalities are localized in any of the walls, which are not seen in this view.

4.3. B-mode (multiplane) parasternal short-axis view

This approach, also referred to as the 'Simpson's method', allows the measurement of ventricular volumes with a higher accuracy by using an approach that bears similarities with the clinical biplane method of disks. In this approach, the total LV volume is calculated from the sum of a stack of elliptical disks. From the parasternal long-axis view, LVEDL and LVESL are measured. Then, images of the LV in its short-axis are analyzed at the following three levels: i) at the level of the base, ii) at an intermediate position, approximately at the level of the papillary muscles, and iii) at the apex level (**Figures 2** and **4**). From these acquisitions, a three-dimensional reconstruction of the LV geometry and the calculation of diastolic and systolic LV volumes are possible using a modified Simpson's rule [36, 81, 82] (also called method disks technique):

$$LVEDV = (A1+A2) \times (LVEDL/3) + (A3/2) \times (LVEDL/3) + (\pi/6) \times (LVEDL/3)^3$$

$$LVESV = (A1+A2) \times (LVESL/3) + (A3/2) \times (LVESL/3) + (\pi/6) \times (LVESL/3)^3$$

where A1, A2, and A3 are LV areas at the level of mitral valve, papillary muscles and apex, in diastole and systole respectively. However, in pathological conditions, e.g. after myocardial infarction, papillary muscles might be either fibrotic and poorly visible or displaced. Thus, an appropriate and consistent method for standardization of the short-axis imaging is warranted. This could be achieved by scrolling along the long-axis to set the basal and apical views at the most distant sections in which the LV chamber is still visible both in systole and diastole (without the inclusion of left atrium at the base) and adding an intermediate recording halfway. Accurate and consistent positioning of the short-axis views is crucial to obtain standardized data, especially in myocardial infarction settings. In each plane, the endocardial border is traced at the end of both diastole and systole, as described above.

Convincing evidence in both humans and rodents [83, 84] has shown that in pathological conditions, such as after myocardial infarction, this method is more accurate to quantify LV volumes and cardiac function compared to the M-mode, due to variable localization and the segmental nature of the ischemic lesion. On the other hand, this method requires adequate acoustic windows for the accurate visualization of the endocardial border and measurement. This is often difficult to achieve in rodents, in which myocardial infarction is mostly induced experimentally by surgical ligation of the proximal left anterior descending (LAD) coronary artery, resulting in apical lesions, which severely affect the definition and resolution of the endocardial border. In addition, the surgical procedure and the sutures on the chest further reduce the quality of the acoustic window and often result in major distortion of the heart's geometry. Thus, to what extent this method is more reliable and accurate compared to the B-mode, single-plane evaluation of the long-axis (in which apical lesions can be better visualized) remains an open question.

4.4. PW Doppler echocardiography

PW Doppler provides hemodynamic information and more precise quantification of SV than 2D echocardiography [85]. In particular, PW Doppler of aortic flow is used to evaluate blood flow velocity at the level of the LV outflow tract (LVOT) to derive the VTI. While LVOT VTI is usually assessed with the five-chamber view, the cross-sectional area is measured with the parasternal long-axis view in B-mode. SV can then be calculated by applying the following equation:

$$SV = VTI \times CSA$$

where CSA refers to the cross-sectional area of the LVOT and can be derived by measuring the LVOT diameter (D) on long-axis parasternal M-mode and assuming its circular shape:

$$CSA = D^2 \times \pi/4 = D^2 \times 0.785$$

Accurate PW Doppler measurements require that US waves are parallel to the blood flow, or that angle correction is implemented when the beam is not aligned with the blood flow. In humans, this is easily achieved by recording a PW Doppler signal at 5 mm from the aortic valve in an apical five-chamber view [85]. In mice, the parallel orientation can be better obtained at the level of the pulmonary artery, as the SV is equal for both ventricles (**Figure 2**). The reliability of PW Doppler echocardiography in determining CO in mice has been validated and compared to standard echocardiography and invasive measurements [86], showing that all US-based techniques tend to overestimate CO. Although B-mode single-plane evaluation provided values which are closely comparable to values derived by invasive assessment, VTI-derived CO assessed at the level of the pulmonary artery was the most reproducible method, showing the lowest interobserver variability. In rats, the approach is the same, but CO can be calculated from CSA and VTIs measured at the LVOT or at the aorta [24].

5. Evaluation of diastolic function

Diastole comprises the relaxation and filling of cardiac cavities to enable an adequate blood volume to maintain normal cardiac output. Diastolic dysfunction can derive from abnormal relaxation and/or increased myocardial stiffness of the LV, eventually leading to elevated LV filling pressures and HF symptoms. In the presence of either preserved or minimally depressed EF, diastolic dysfunction is the main determinant of HFpEF. Assessment of diastolic dysfunction is receiving more and more attention, as HFpEF currently accounts for nearly half of the HF patients, and its prevalence continues to rise due to the increasingly aged society and survival of patients with comorbidities for HFpEF, such as type 2 diabetes, hypertension, and obesity[87]. While the prevalence of HFpEF rises, no effective therapeutic and prevention options are available, mostly due to a lack of pathophysiological understanding, patient heterogeneity, and underdiagnosis [88, 89]. Diastolic dysfunction is frequently associated with increased interstitial fibrosis, LV concentric hypertrophy, and atrial enlargement. Moreover, pulmonary hypertension and RV dysfunction, often arising in response to elevated LV filling pressure, are key hemodynamic abnormalities in diastolic dysfunction, which can effectively stratify HF phenotypes (with both reduced and preserved EF) [90, 91].

As in humans, assessment of LV diastolic function in rodents includes Doppler evaluation of LV filling velocity, measured by the ratio between early (E) and late (A) diastolic transmitral Doppler flow velocities (E/A), isovolumetric relaxation time (IVRT), mitral valve E wave deceleration time (DT), and LA area [92]. Nevertheless, E/A and IVRT are highly dependent on the pressure gradient between left atrium and ventricle. With the emergence of TDI, myocardial motion in early diastole, as assessed by peak early-diastolic annular velocity (e’), became a good measure of diastolic function [24]. E to e’ ratio is, therefore, an appropriate estimator of LV filling pressures, that has been adopted as one of the criteria for clinical diagnosis of HFpEF and is successfully applied in small animal studies [92]. Lately, the E-wave deceleration rate E/DT has been proposed, outperforming the tissue Doppler-derived index E/e' in characterizing lung remodeling in HFpEF [93].

While most of the indexes of diastolic function are relatively easy to obtain in rats, their measurement requires expert training in mice with their higher HR and smaller heart size. The same distinction applies for normal cut-off values, which appear highly variable in intra- and inter-strain comparative studies in mice [94]. Conversely, reference values appear more homogeneous and standardized in rats (**Table 1**) [95, 96]. Finally, while in humans, echocardiographic diastolic parameters have been clinically and hemodynamically validated, with E/e' ratio values > 15 consistently associated with elevated LV filling pressures, this evidence has only recently been provided for rats [97] and is still not reported for mice. While most studies provide "normal" E/e' ratio values between 20 and 30 [98-100], it has to be emphasized that, in mice, it is very difficult to measure e' velocity close to the mitral valve, often resulting in its underestimation (**Figure 3**).

In view of these limitations, the following guidelines will be useful to standardize the evaluation of diastolic function and define universal reference values also in mice.

5.1. B-mode, apical four-chamber evaluation

Analysis of diastolic function should start with the B-mode to visualize the apical four-chamber view. Although the LA area can be measured in parasternal long-axis orientation, we recommend measuring it in the four-chamber view in B-Mode, assuring the simultaneous visualization of atria as well as mitral and tricuspid valves opening and closing (**Figure 2**). LA maximal extension should be confirmed by observing cine-loop recordings. Indeed, the LA area has been routinely used as a marker for chronic elevation of LV filling pressure and diastolic dysfunction in both humans and animal models [92, 101].

Apart from diastole, if one aims to evaluate valvular function, this plane also allows a suitable alignment of mitral and tricuspid annuli to assess their motion in M-mode. Slightly tilting the transducer down enables a five-chamber view, where the left ventricular outflow tract and aorta are revealed (**Figure 2**).

5.2. PW and Tissue Doppler in apical four-chamber evaluation

The apical four-chamber view represents the preferred plane for recording transmitral Doppler flows (E and A velocities, their ratio, DT, and IVRT) and TDI imaging (e', a', and s') with the sample volume placed at the tips of the mitral leaflet and at the lateral mitral valve annulus, respectively. The E wave represents the transmitral blood flow during the LV early filling phase and can be affected by the rate of LV relaxation and its compliance. The A wave represents the transmitral blood flow during the atrial contraction phase and can be altered by LA contractility or compliance [102]. The E/A ratio provides important information about LV filling dynamics [24]. Special attention should be given when assessing these velocities, as they are highly dependent on HR, and thus anesthesia. Preferentially, these measurements should be acquired with other more reliable parameters, such as annular tissue velocities and LA size [102]. Other diastolic parameters include DT, the duration of E wave peak to the baseline, and IVRT, which is the time from the closure of the aortic valve to the opening of the mitral valve. Increased IVRT and DT reflect a prolonged LV relaxation, but can both be influenced by a number of factors, such as preload, arrhythmia or very high HR, as well as diseases that cause hyperdynamic states.

During TDI, early (e') and late (a') diastolic mitral annulus peak velocity and systolic peak wave can be assessed. The e' velocity is determined by LV relaxation, restoring forces, and filling pressures. e' velocity has been shown to correlate well with invasive measures of IVRT constant of myocardial relaxation, tau [103]. The mitral E/e' is proposed to reflect LA pressure, and, indirectly, LV end-diastolic pressure. The E/e' is less sensitive to preload than other echocardiographic indexes of diastolic function [104]. Currently, an elevated E/e' is proposed as a guideline for the diagnosis of diastolic dysfunction [105]. However, under certain conditions, including (i) tachycardia with fusion of E and A velocities, (ii) unreliable measurement of E velocity (significant mitral regurgitation), (iii) unreliable e' velocities (e.g. mitral valve replacement, mitral annular calcification, mitral stenosis, and/or left bundle branch block), and/or (iv) significant aortic regurgitation, precautions should be taken with regard to the use of E/e' as a marker for diastolic dysfunction [106]. For the acquisition of TDI, the gain should be considerably adjusted to avoid superimposition of multiple amplitudes. Furthermore, it is important to position the sample volume at the myocardium, as close as possible to the mitral or tricuspid annuli to assess the areas with greater excursion enabling the recording of maximal velocities with a better temporal resolution [24]. Measurements acquired in myocardial areas distal to the ones herein recommended will result in lower velocities and increased E/e' values (**Figure 3**).

At heart rates > 450 bpm, E and A waves are frequently merged. Some authors suggest to artificially reduce heart rate by increasing anesthesia proportionally in all groups. We argue that this is not physiological and should be avoided. Instead, one should try to extract E-wave velocity peak value and normalize it to e'. Indeed, E/e' represents a much more reliable parameter to assess diastolic function when compared to E/A, since it has an excellent correlation with LV end-diastolic pressure (LVEDP, indicative of myocardial stiffness) and tau [23, 94, 103]. Other echocardiographic indexes have been proposed as surrogates of LVEDP, such as E/DT, after normalizing DT to cardiac cycle duration [97].

Both PW and TDI allow extracting the values of isovolumetric contraction time (IVCT), IVRT and ejection time (ET) as shown in **Figure 2**. From these, one can derive Myocardial Performance Index (TEI Index) [107]:

$$\text{TEI} = (\text{IVCT} + \text{IVRT}) / \text{ET}$$

We should emphasize that while IVRT is a diastolic parameter, TEI index assesses myocardial global function, including both diastolic and systolic function. The underlying rationale is that both isovolumetric periods, IVRT and IVCT, are energy-dependent but do not produce work. Myocardial dysfunction usually prolongs the isovolumetric periods, yielding higher values for this index compared to a healthy heart.

Finally, as mentioned earlier, several studies have established an independent relationship between RV dysfunction and the prevalence and prognosis of HFpEF, using feasible and readily available echocardiographic measurements [90, 91]. Tricuspid annular plane systolic excursion (TAPSE) reproduces well the degree of RV longitudinal contraction and has proven to be a reliable parameter to assess global RV function (**Figure 2**). TAPSE is measured in the apical four-chamber view and the M-mode cursor should be positioned on the lateral tricuspid annulus near the free RV wall and aligned as close as possible to the apex of the heart. Special care should be taken in assuring the RV is clearly visualized in the M-mode view. Maximal TAPSE is defined by the total excursion/distance between the ventricle end-diastole and end-systole [108].

6. Assessment of LV function in animal models of disease

A brief description of the echocardiographic views, modalities and derived parameters for common cardiovascular diseases, including chronic pressure overload, myocardial infarction and diastolic dysfunction associated to HFpEF, is provided in **Table 3**. Representative images of hearts affected by chronic pressure-overload and myocardial infarction, in comparison to normal, healthy hearts, are provided in **Figure 4**. In diseased conditions, the echocardiographic examination may be limited by poor window size and image acquisition due to the positioning of the ribs or to the presence of abundant fat tissue inside and around the thoracic cavity. Indeed, fat is very echogenic, i.e. US are easily reflected, attenuated and slowed down through the fat layer, which impairs the quality of the images. In addition, anesthetic induction and maintenance can vary significantly due to adiposity, causing differential degrees of cardio-depression.

As mentioned above, surgical models require the use of sutures that significantly compromise the quality of the acoustic windows. Post-intervention fibrosis may accumulate around the heart further diminishing the quality of the echocardiographic images. In addition, fibrosis can induce a slight rotation or distortion of the heart, which may demand a corresponding corrective rotation of the transducer.

Despite these limitations, echocardiography remains an invaluable tool to assess LV function in animal models of human diseases, that follows the principles of the 3Rs (refine, reduce and replace). Furthermore, it allows assessing longitudinal progression over time, i.e. at different ages in the same animal, as it is neither painful nor invasive (as compared to pressure/volume loop method for example), and therefore suitable to refine and reduce the number of studied animals. Moreover, as it has an extensive application in human diagnostics, echocardiography is a continuously evolving technique.

7. Data analysis

When analyzing echocardiographic data, one should:

1. Register anesthetic parameters.
2. Acquire and analyze data blindly (as echocardiographic analysis is subjective and researcher-dependent, the data should be analyzed by multiple researchers and averages should be recorded).
3. Record and present HR.
4. Extract diastolic and systolic volumes from the same cardiac cycle.
5. Average measurements from at least three different cycles.
6. Calculate indexed values whenever the animals show large differences in BW (CI, EDV and ESV). In this case, values should be normalized to BSA defined as $9.8*BW^{2/3}$ [79, 80]. This applies mostly to volumes, dimensions and LV mass.
7. Record and store measurements as well as cine-loop recordings. Ensure that a working-station is available to analyze the data off-line, without occupying the equipment.

8. Conclusions

Echocardiography is not an automated procedure and it is highly operator-dependent, relying on a proper acquisition and interpretation of the results by an examiner who is familiarized with both its capabilities and its limitations. We believe therefore that some minimal requirements need to be defined and followed by experimental researchers to increase the reliability of the data reported in publications and to allow a better comparison of studies performed in different laboratories.

This paper provides a list of standards, which should be met in order to evaluate LV function in rodents. We also provide a list of common pitfalls during basic echocardiographic examination (**Figure 3**). Briefly, animals should be sedated with the minimal dose of anesthesia, whenever possible through inhaled halogenated gases, keeping the core body temperature around 37°C and HR above 350 bpm in rats and 450 bpm in mice. In any case, the name and dose/concentration of the anesthetic, the HR and the body temperature should be clearly indicated.

Systolic function should be assessed on B-mode images, using either single- or multi-plane evaluation. Experimental studies comparing the efficacy of these two methods in estimating cardiac volumes, as precisely determined by invasive hemodynamic monitoring, are highly encouraged and should provide a definitive answer regarding the optimal method to be followed in diverse models of heart disease (i.e. segmental versus global systolic dysfunction). In any case, a detailed description of the method used to calculate systolic function must be provided. M-mode evaluation should be limited to LV diameters and FS. Volume extrapolation is not accurate and should therefore be discouraged when evaluating systolic function, as already repeatedly recommended in clinical use [40, 109]. Analysis should, preferentially, be performed post-acquisition by blinded operators, and the measures to ensure blinding should be clearly indicated.

Diastolic function should be evaluated on B-mode images, mostly using the apical four-chamber view. Analysis should start by measuring LA area, followed by recording transmitral PW Doppler flows and TDI imaging to obtain E/A, E/e’, IVRT and DT values. Of these, enlarged LA size (in both mice and rats) and increased E/e’ (in rats) appear as the most reliable parameters to indicate elevated LV filling pressures. As in humans, diastolic dysfunction in rodents should be determined and proven by simultaneous alteration of multiple indexes, although definitive cut-off values still need to be determined.

In addition to these methodological standards, more active interaction and discussion between experimental researchers and clinical sonographers should be encouraged to increase awareness of the morphological features of the heart in healthy and diseased conditions, as well as to import the most recent advances in echocardiographic tools and software to laboratory settings. Standardization of echocardiography, a non-invasive, inexpensive, widely available, and repeatable technique, would likely improve the translation from small animals to the clinic. Furthermore, as patients are often diagnosed once they have an established disease, standardization of echocardiography could help to find earlier characteristics of disease, which would improve the diagnosis at an earlier stage in humans.

Various publications and databases are available and provide reference values for echocardiography measurements and calculations derived from different strains and genders of mice and rats [28, 110-112]. As these normal values have not been obtained using a standardized approach, **Tables 1** and **2** provide a summary of reference values obtained in our laboratories, following the recommendations listed in this manuscript, for the most commonly used rodent strains and anesthetics. Inexperienced sonographers are encouraged to refer to these data to match the experimental results for control animals and ensure sufficient data reliability.

Acknowledgements

This work was supported by AIRC IG grant 2016 19032 to S.Z.; FEDER through Compete 2020 – Programa Operacional Competitividade E Internacionalização (POCI), the project DOCNET (norte-01-0145-feder-000003), supported by Norte Portugal regional operational programme (norte 2020), under the Portugal 2020 partnership agreement, through the European Regional Development Fund (ERDF), the project NETDIAMOND (POCI-01-0145-FEDER-016385), supported by European Structural And Investment Funds, Lisbon's regional operational program 2020 to I.P.F.; grants from FSR-FNRS, FRC (Cliniques Universitaires Saint-Luc) and from Action de Recherche Concertée (UCLouvain) to C.B., E.P.D. and L.B; the ERA-Net-CVD project MacroERA, 01KL1706, FP7-Homage N° 305507, and IMI2-CARDIATEAM (N° 821508) to S.H., the DZHK (German Centre for Cardiovascular Research) and the German Ministry of Research and Education (BMBF) to F.W., T.E. and L.C., the Netherlands Cardiovascular Research Initiative, an initiative with support of the Dutch Heart Foundation, CVON2016-Early HFPEF, 2015-10, CVON She-PREDICTS, grant 2017-21, CVON Arena-PRIME, 2017-18, Flemish Research Foundation FWO G091018N and FWO G0B5930N to S.H.; Federico II University/Ricerca di Ateneo grant to C.G..T.; the European Research Area Networks on Cardiovascular Diseases (ERA-CVD) [LYMIT-DIS 2016, MacroERA], Fonds Wetenschappelijk Onderzoek [1160718N] to I.C; the Deutsche Forschungsgemeinschaft (DFG TH903/20-1, KFO311), the Transregio-SFB INST 95/15641 and the EU Horizon 2020 project Cardioregenix (GA 825670) to T.T.

Conflict of interest

T.T. is founder and shareholder of Cardior Pharmaceuticals GmbH.

References

1. Knoll R, Iaccarino G, Tarone G, Hilfiker-Kleiner D, Bauersachs J, Leite-Moreira AF, Sugden PH, Balligand JL, European Society of C. Towards a re-definition of 'cardiac hypertrophy' through a rational characterization of left ventricular phenotypes: a position paper of the Working Group 'Myocardial Function' of the ESC. *Eur J Heart Fail* 2011;**13**:811-819.
2. Houser SR, Margulies KB, Murphy AM, Spinale FG, Francis GS, Prabhu SD, Rockman HA, Kass DA, Molkentin JD, Sussman MA, Koch WJ, American Heart Association Council on Basic Cardiovascular Sciences CoCC, Council on Functional G, Translational B. Animal models of heart failure: a scientific statement from the American Heart Association. *Circ Res* 2012;**111**:131-150.
3. Kimmelman J, Federico C. Consider drug efficacy before first-in-human trials. *Nature* 2017;**542**:25-27.
4. Perrin S. Preclinical research: Make mouse studies work. *Nature* 2014;**507**:423-425.
5. Jabs M, Rose AJ, Lehmann LH, Taylor J, Moll I, Sijmonsma TP, Herberich SE, Sauer SW, Poschet G, Federico G, Mogler C, Weis EM, Augustin HG, Yan M, Gretz N, Schmid RM, Adams RH, Grone HJ, Hell R, Okun JG, Backs J, Nawroth PP, Herzig S, Fischer A. Inhibition of Endothelial Notch Signaling Impairs Fatty Acid Transport and Leads to Metabolic and Vascular Remodeling of the Adult Heart. *Circulation* 2018.
6. Ong SG, Lee WH, Huang M, Dey D, Kodo K, Sanchez-Freire V, Gold JD, Wu JC. Cross talk of combined gene and cell therapy in ischemic heart disease: role of exosomal microRNA transfer. *Circulation* 2014;**130**:S60-69.
7. Wang H, Xu X, Fassett J, Kwak D, Liu X, Hu X, Falls TJ, Bell JC, Li H, Bitterman P, Bache RJ, Chen Y. Double-stranded RNA-dependent protein kinase deficiency protects the heart from systolic overload-induced congestive heart failure. *Circulation* 2014;**129**:1397-1406.
8. Boon RA, Iekushi K, Lechner S, Seeger T, Fischer A, Heydt S, Kaluza D, Treguer K, Carmona G, Bonauer A, Horrevoets AJ, Didier N, Girmatsion Z, Biliczki P, Ehrlich JR, Katus HA, Muller OJ, Potente M, Zeiher AM, Hermeking H, Dimmeler S. MicroRNA-34a regulates cardiac ageing and function. *Nature* 2013;**495**:107-110.
9. Lindsey ML, Bolli R, Canty JM, Jr., Du XJ, Frangogiannis NG, Frantz S, Gourdie RG, Holmes JW, Jones SP, Kloner RA, Lefer DJ, Liao R, Murphy E, Ping P, Przyklenk K, Recchia FA, Schwartz Longacre L, Ripplinger CM, Van Eyk JE, Heusch G. Guidelines for experimental models of myocardial ischemia and infarction. *Am J Physiol Heart Circ Physiol* 2018;**314**:H812-H838.
10. Lindsey ML, Kassiri Z, Virag JAI, de Castro Bras LE, Scherrer-Crosbie M. Guidelines for measuring cardiac physiology in mice. *Am J Physiol Heart Circ Physiol* 2018;**314**:H733-H752.
11. Pachon RE, Scharf BA, Vatner DE, Vatner SF. Best anesthetics for assessing left ventricular systolic function by echocardiography in mice. *Am J Physiol Heart Circ Physiol* 2015;**308**:H1525-1529.
12. Donner DG, Kiriazis H, Du XJ, Marwick TH, McMullen JR. Improving the quality of preclinical research echocardiography: observations, training, and guidelines for measurement. *Am J Physiol Heart Circ Physiol* 2018;**315**:H58-H70.
13. Gardin JM, Siri FM, Kitsis RN, Edwards JG, Leinwand LA. Echocardiographic assessment of left ventricular mass and systolic function in mice. *Circ Res* 1995;**76**:907-914.
14. Phoon CK, Turnbull DH. Cardiovascular Imaging in Mice. *Curr Protoc Mouse Biol* 2016;**6**:15-38.
15. Ram R, Mickelsen DM, Theodoropoulos C, Blaxall BC. New approaches in small animal echocardiography: imaging the sounds of silence. *Am J Physiol Heart Circ Physiol* 2011;**301**:H1765-1780.
16. Scherrer-Crosbie M, Thibault HB. Echocardiography in translational research: of mice and men. *J Am Soc Echocardiogr* 2008;**21**:1083-1092.
17. Bauer M, Cheng S, Jain M, Ngoy S, Theodoropoulos C, Trujillo A, Lin FC, Liao R. Echocardiographic speckle-tracking based strain imaging for rapid cardiovascular phenotyping in mice. *Circ Res* 2011;**108**:908-916.
18. Gao S, Ho D, Vatner DE, Vatner SF. Echocardiography in Mice. *Curr Protoc Mouse Biol* 2011;**1**:71-83.
19. Yang XP, Liu YH, Rhaleb NE, Kurihara N, Kim HE, Carretero OA. Echocardiographic assessment of cardiac function in conscious and anesthetized mice. *Am J Physiol* 1999;**277**:H1967-1974.
20. Janssen BJ, De Celle T, Debets JJ, Brouns AE, Callahan MF, Smith TL. Effects of anesthetics on systemic hemodynamics in mice. *Am J Physiol Heart Circ Physiol* 2004;**287**:H1618-1624.
21. Patel HH, Ludwig LM, Fryer RM, Hsu AK, Warltier DC, Gross GJ. Delta opioid agonists and volatile anesthetics facilitate cardioprotection via potentiation of K(ATP) channel opening. *FASEB J* 2002;**16**:1468-1470.
22. Tanaka K, Ludwig LM, Kersten JR, Pagel PS, Warltier DC. Mechanisms of cardioprotection by volatile anesthetics. *Anesthesiology* 2004;**100**:707-721.
23. Roth DM, Swaney JS, Dalton ND, Gilpin EA, Ross J, Jr. Impact of anesthesia on cardiac function during echocardiography in mice. *Am J Physiol Heart Circ Physiol* 2002;**282**:H2134-2140.
24. Lourenço A, I F-P, AF L-M. In vivo Experimental Assessment of Cardiac Function. In: DV C, ed. Introduction to Translational Cardiovascular Research: Springer International Switzerland, 2014:389-411.

25. Wilding LA, Hampel JA, Khoury BM, Kang S, Machado-Aranda D, Raghavendran K, Nemzek JA. Benefits of 21% Oxygen Compared with 100% Oxygen for Delivery of Isoflurane to Mice (Mus musculus) and Rats (Rattus norvegicus). *J Am Assoc Lab Anim Sci* 2017;**56**:148-154.
26. Constantinides C, Murphy K. Molecular and Integrative Physiological Effects of Isoflurane Anesthesia: The Paradigm of Cardiovascular Studies in Rodents using Magnetic Resonance Imaging. *Front Cardiovasc Med* 2016;**3**:23.
27. Riou B, Viars P, Lecarpentier Y. Effects of ketamine on the cardiac papillary muscle of normal hamsters and those with cardiomyopathy. *Anesthesiology* 1990;**73**:910-918.
28. Redfors B, Shao Y, Omerovic E. Influence of anesthetic agent, depth of anesthesia and body temperature on cardiovascular functional parameters in the rat. *Lab Anim* 2014;**48**:6-14.
29. Sano Y, Ito S, Yoneda M, Nagasawa K, Matsuura N, Yamada Y, Uchinaka A, Bando YK, Murohara T, Nagata K. Effects of various types of anesthesia on hemodynamics, cardiac function, and glucose and lipid metabolism in rats. *Am J Physiol Heart Circ Physiol* 2016;**311**:H1360-H1366.
30. Stein AB, Tiwari S, Thomas P, Hunt G, Levent C, Stoddard MF, Tang XL, Bolli R, Dawn B. Effects of anesthesia on echocardiographic assessment of left ventricular structure and function in rats. *Basic Res Cardiol* 2007;**102**:28-41.
31. Campen MJ, Tagaito Y, Jenkins TP, Balbir A, O'Donnell CP. Heart rate variability responses to hypoxic and hypercapnic exposures in different mouse strains. *J Appl Physiol (1985)* 2005;**99**:807-813.
32. Doevendans PA, Daemen MJ, de Muinck ED, Smits JF. Cardiovascular phenotyping in mice. *Cardiovasc Res* 1998;**39**:34-49.
33. Mattson DL. Comparison of arterial blood pressure in different strains of mice. *Am J Hypertens* 2001;**14**:405-408.
34. Respress JL, Wehrens XH. Transthoracic echocardiography in mice. *J Vis Exp* 2010.
35. Picard MH, Adams D, Bierig SM, Dent JM, Douglas PS, Gillam LD, Keller AM, Malenka DJ, Masoudi FA, McCulloch M, Pellikka PA, Peters PJ, Stainback RF, Strachan GM, Zoghbi WA, American Society of E. American Society of Echocardiography recommendations for quality echocardiography laboratory operations. *J Am Soc Echocardiogr* 2011;**24**:1-10.
36. Folland ED, Parisi AF, Moynihan PF, Jones DR, Feldman CL, Tow DE. Assessment of left ventricular ejection fraction and volumes by real-time, two-dimensional echocardiography. A comparison of cineangiographic and radionuclide techniques. *Circulation* 1979;**60**:760-766.
37. Leitman M, Lysyansky P, Sidenko S, Shir V, Peleg E, Binenbaum M, Kaluski E, Krakover R, Vered Z. Two-dimensional strain-a novel software for real-time quantitative echocardiographic assessment of myocardial function. *J Am Soc Echocardiogr* 2004;**17**:1021-1029.
38. Voigt JU, Pedrizzetti G, Lysyansky P, Marwick TH, Houle H, Baumann R, Pedri S, Ito Y, Abe Y, Metz S, Song JH, Hamilton J, Sengupta PP, Kolias TJ, d'Hooge J, Aurigemma GP, Thomas JD, Badano LP. Definitions for a common standard for 2D speckle tracking echocardiography: consensus document of the EACVI/ASE/Industry Task Force to standardize deformation imaging. *Eur Heart J Cardiovasc Imaging* 2015;**16**:1-11.
39. Collier P, Phelan D, Klein A. A Test in Context: Myocardial Strain Measured by Speckle-Tracking Echocardiography. *J Am Coll Cardiol* 2017;**69**:1043-1056.
40. Lang RM, Badano LP, Mor-Avi V, Afilalo J, Armstrong A, Ernande L, Flachskampf FA, Foster E, Goldstein SA, Kuznetsova T, Lancellotti P, Muraru D, Picard MH, Rietzschel ER, Rudski L, Spencer KT, Tsang W, Voigt JU. Recommendations for cardiac chamber quantification by echocardiography in adults: an update from the American Society of Echocardiography and the European Association of Cardiovascular Imaging. *Eur Heart J Cardiovasc Imaging* 2015;**16**:233-270.
41. Biering-Sorensen T, Hoffmann S, Mogelvang R, Zeeberg Iversen A, Galatius S, Fritz-Hansen T, Bech J, Jensen JS. Myocardial strain analysis by 2-dimensional speckle tracking echocardiography improves diagnostics of coronary artery stenosis in stable angina pectoris. *Circ Cardiovasc Imaging* 2014;**7**:58-65.
42. Gjesdal O, Vartdal T, Hopp E, Lunde K, Brunvand H, Smith HJ, Edvardsen T. Left ventricle longitudinal deformation assessment by mitral annulus displacement or global longitudinal strain in chronic ischemic heart disease: are they interchangeable? *J Am Soc Echocardiogr* 2009;**22**:823-830.
43. Nucifora G, Schuijf JD, Delgado V, Bertini M, Scholte AJ, Ng AC, van Werkhoven JM, Jukema JW, Holman ER, van der Wall EE, Bax JJ. Incremental value of subclinical left ventricular systolic dysfunction for the identification of patients with obstructive coronary artery disease. *Am Heart J* 2010;**159**:148-157.
44. Vartdal T, Brunvand H, Pettersen E, Smith HJ, Lyseggen E, Helle-Valle T, Skulstad H, Ihlen H, Edvardsen T. Early prediction of infarct size by strain Doppler echocardiography after coronary reperfusion. *J Am Coll Cardiol* 2007;**49**:1715-1721.
45. Bhan A, Sirker A, Zhang J, Protti A, Catibog N, Driver W, Botnar R, Monaghan MJ, Shah AM. High-frequency speckle tracking echocardiography in the assessment of left ventricular function and remodeling after murine myocardial infarction. *Am J Physiol Heart Circ Physiol* 2014;**306**:H1371-1383.

46. Kraigher-Krainer E, Shah AM, Gupta DK, Santos A, Claggett B, Pieske B, Zile MR, Voors AA, Lefkowitz MP, Packer M, McMurray JJ, Solomon SD, Investigators P. Impaired systolic function by strain imaging in heart failure with preserved ejection fraction. *J Am Coll Cardiol* 2014;**63**:447-456.
47. Popovic ZB, Kwon DH, Mishra M, Buakhamsri A, Greenberg NL, Thamilarasan M, Flamm SD, Thomas JD, Lever HM, Desai MY. Association between regional ventricular function and myocardial fibrosis in hypertrophic cardiomyopathy assessed by speckle tracking echocardiography and delayed hyperenhancement magnetic resonance imaging. *J Am Soc Echocardiogr* 2008;**21**:1299-1305.
48. Reant P, Mirabel M, Lloyd G, Peyrou J, Lopez Ayala JM, Dickie S, Bulluck H, Captur G, Rosmini S, Guttmann O, Demetrescu C, Pantazis A, Tome-Esteban M, Moon JC, Lafitte S, McKenna WJ. Global longitudinal strain is associated with heart failure outcomes in hypertrophic cardiomyopathy. *Heart* 2016;**102**:741-747.
49. An X, Wang J, Li H, Lu Z, Bai Y, Xiao H, Zhang Y, Song Y. Speckle Tracking Based Strain Analysis Is Sensitive for Early Detection of Pathological Cardiac Hypertrophy. *PLoS One* 2016;**11**:e0149155.
50. Coppola C, Riccio G, Barbieri A, Monti MG, Piscopo G, Rea D, Arra C, Maurea C, De Lorenzo C, Maurea N. Antineoplastic-related cardiotoxicity, morphofunctional aspects in a murine model: contribution of the new tool 2D-speckle tracking. *Onco Targets Ther* 2016;**9**:6785-6794.
51. Hare JL, Brown JK, Leano R, Jenkins C, Woodward N, Marwick TH. Use of myocardial deformation imaging to detect preclinical myocardial dysfunction before conventional measures in patients undergoing breast cancer treatment with trastuzumab. *Am Heart J* 2009;**158**:294-301.
52. Plana JC, Galderisi M, Barac A, Ewer MS, Ky B, Scherrer-Crosbie M, Ganame J, Sebag IA, Agler DA, Badano LP, Banchs J, Cardinale D, Carver J, Cerqueira M, DeCara JM, Edvardsen T, Flamm SD, Force T, Griffin BP, Jerusalem G, Liu JE, Magalhaes A, Marwick T, Sanchez LY, Sicari R, Villarraga HR, Lancellotti P. Expert consensus for multimodality imaging evaluation of adult patients during and after cancer therapy: a report from the American Society of Echocardiography and the European Association of Cardiovascular Imaging. *J Am Soc Echocardiogr* 2014;**27**:911-939.
53. Rea D, Coppola C, Barbieri A, Monti MG, Misso G, Palma G, Bimonte S, Zarone MR, Luciano A, Liccardo D, Maiolino P, Cittadini A, Ciliberto G, Arra C, Maurea N. Strain Analysis in the Assessment of a Mouse Model of Cardiotoxicity due to Chemotherapy: Sample for Preclinical Research. *In Vivo* 2016;**30**:279-290.
54. van der Bijl P, Bootsma M, Hiemstra YL, Ajmone Marsan N, Bax JJ, Delgado V. Left ventricular 2D speckle tracking echocardiography for detection of systolic dysfunction in genetic, dilated cardiomyopathies. *Eur Heart J Cardiovasc Imaging* 2019;**20**:694-699.
55. Verdonschot JAJ, Merken JJ, Brunner-La Rocca HP, Hazebroek MR, Eurlings C, Thijssen E, Wang P, Weerts J, van Empel V, Schummers G, Schreckenberg M, van den Wijngaard A, Lumens J, Brunner HG, Heymans SRB, Krapels IPC, Knackstedt C. Value of Speckle Tracking-Based Deformation Analysis in Screening Relatives of Patients Asymptomatic Dilated Cardiomyopathy. *JACC Cardiovasc Imaging* 2019.
56. Schafer S, Viswanathan S, Widjaja AA, Lim WW, Moreno-Moral A, DeLaughter DM, Ng B, Patone G, Chow K, Khin E, Tan J, Chothani SP, Ye L, Rackham OJL, Ko NSJ, Sahib NE, Pua CJ, Zhen NTG, Xie C, Wang M, Maatz H, Lim S, Saar K, Blachut S, Petretto E, Schmidt S, Putoczki T, Guimaraes-Camboa N, Wakimoto H, van Heesch S, Sigmundsson K, Lim SL, Soon JL, Chao VTT, Chua YL, Tan TE, Evans SM, Loh YJ, Jamal MH, Ong KK, Chua KC, Ong BH, Chakaramakkil MJ, Seidman JG, Seidman CE, Hubner N, Sin KYK, Cook SA. IL-11 is a crucial determinant of cardiovascular fibrosis. *Nature* 2017;**552**:110-115.
57. Leach JP, Heallen T, Zhang M, Rahmani M, Morikawa Y, Hill MC, Segura A, Willerson JT, Martin JF. Hippo pathway deficiency reverses systolic heart failure after infarction. *Nature* 2017;**550**:260-264.
58. Nakada Y, Canseco DC, Thet S, Abdisalaam S, Asaithamby A, Santos CX, Shah AM, Zhang H, Faber JE, Kinter MT, Szweda LI, Xing C, Hu Z, Deberardinis RJ, Schiattarella G, Hill JA, Oz O, Lu Z, Zhang CC, Kimura W, Sadek HA. Hypoxia induces heart regeneration in adult mice. *Nature* 2017;**541**:222-227.
59. Li M, Sala V, De Santis MC, Cimino J, Cappello P, Pianca N, Di Bona A, Margaria JP, Martini M, Lazzarini E, Pirozzi F, Rossi L, Franco I, Bornbaum J, Heger J, Rohrbach S, Perino A, Tocchetti CG, Lima BHF, Teixeira MM, Porporato PE, Schulz R, Angelini A, Sandri M, Ameri P, Sciarretta S, Lima-Junior RCP, Mongillo M, Zaglia T, Morello F, Novelli F, Hirsch E, Ghigo A. Phosphoinositide 3-Kinase Gamma Inhibition Protects from Anthracycline Cardiotoxicity and Reduces Tumor Growth. *Circulation* 2018.
60. Ruozi G, Bortolotti F, Falcione A, Dal Ferro M, Ukovich L, Macedo A, Zentilin L, Filigheddu N, Gortan Cappellari G, Baldini G, Zweyer M, Barazzoni R, Graziani A, Zacchigna S, Giacca M. AAV-mediated in vivo functional selection of tissue-protective factors against ischaemia. *Nat Commun* 2015;**6**:7388.
61. Barefield DY, Puckelwartz MJ, Kim EY, Wilsbacher LD, Vo AH, Waters EA, Earley JU, Hadhazy M, Dellefave-Castillo L, Pesce LL, McNally EM. Experimental Modeling Supports a Role for MyBP-HL as a Novel Myofilament Component in Arrhythmia and Dilated Cardiomyopathy. *Circulation* 2017;**136**:1477-1491.

62. Cameron SJ, Ture SK, Mickelsen D, Chakrabarti E, Modjeski KL, McNitt S, Seaberry M, Field DJ, Le NT, Abe J, Morrell CN. Platelet Extracellular Regulated Protein Kinase 5 Is a Redox Switch and Triggers Maladaptive Platelet Responses and Myocardial Infarct Expansion. *Circulation* 2015;**132**:47-58.
63. Wang WE, Li L, Xia X, Fu W, Liao Q, Lan C, Yang D, Chen H, Yue R, Zeng C, Zhou L, Zhou B, Duan DD, Chen X, Houser SR, Zeng C. Dedifferentiation, Proliferation, and Redifferentiation of Adult Mammalian Cardiomyocytes After Ischemic Injury. *Circulation* 2017;**136**:834-848.
64. Eulalio A, Mano M, Dal Ferro M, Zentilin L, Sinagra G, Zacchigna S, Giacca M. Functional screening identifies miRNAs inducing cardiac regeneration. *Nature* 2012;**492**:376-381.
65. Lesizza P, Merlo M, Vitrella G, Sinagra G. Hypertrophic restrictive cardiomyopathy with apical thinning: a peculiar case of genotype-phenotype correlation. *J Cardiovasc Med (Hagerstown)* 2017;**18**:835-836.
66. Wei K, Serpooshan V, Hurtado C, Diez-Cunado M, Zhao M, Maruyama S, Zhu W, Fajardo G, Noseda M, Nakamura K, Tian X, Liu Q, Wang A, Matsuura Y, Bushway P, Cai W, Savchenko A, Mahmoudi M, Schneider MD, van den Hoff MJ, Butte MJ, Yang PC, Walsh K, Zhou B, Bernstein D, Mercola M, Ruiz-Lozano P. Epicardial FSTL1 reconstitution regenerates the adult mammalian heart. *Nature* 2015;**525**:479-485.
67. Mor-Avi V, Lang RM, Badano LP, Belohlavek M, Cardim NM, Derumeaux G, Galderisi M, Marwick T, Nagueh SF, Sengupta PP, Sicari R, Smiseth OA, Smulevitz B, Takeuchi M, Thomas JD, Vannan M, Voigt JU, Zamorano JL. Current and evolving echocardiographic techniques for the quantitative evaluation of cardiac mechanics: ASE/EAE consensus statement on methodology and indications endorsed by the Japanese Society of Echocardiography. *Eur J Echocardiogr* 2011;**12**:167-205.
68. Dawson D, Lygate CA, Saunders J, Schneider JE, Ye X, Hulbert K, Noble JA, Neubauer S. Quantitative 3-dimensional echocardiography for accurate and rapid cardiac phenotype characterization in mice. *Circulation* 2004;**110**:1632-1637.
69. Grune J, Blumrich A, Brix S, Jeuthe S, Drescher C, Grune T, Foryst-Ludwig A, Messroghli D, Kuebler WM, Ott C, Kintscher U. Evaluation of a commercial multi-dimensional echocardiography technique for ventricular volumetry in small animals. *Cardiovasc Ultrasound* 2018;**16**:10.
70. Mearini G, Stimpel D, Kramer E, Geertz B, Braren I, Gedicke-Hornung C, Precigout G, Muller OJ, Katus HA, Eschenhagen T, Voit T, Garcia L, Lorain S, Carrier L. Repair of Mybpc3 mRNA by 5'-trans-splicing in a Mouse Model of Hypertrophic Cardiomyopathy. *Mol Ther Nucleic Acids* 2013;**2**:e102.
71. Zentilin L, Puligadda U, Lionetti V, Zacchigna S, Collesi C, Pattarini L, Ruozi G, Camporesi S, Sinagra G, Pepe M, Recchia FA, Giacca M. Cardiomyocyte VEGFR-1 activation by VEGF-B induces compensatory hypertrophy and preserves cardiac function after myocardial infarction. *FASEB J* 2010;**24**:1467-1478.
72. Moran CM, Thomson AJ, Rog-Zielinska E, Gray GA. High-resolution echocardiography in the assessment of cardiac physiology and disease in preclinical models. *Exp Physiol* 2013;**98**:629-644.
73. Sahn DJ, DeMaria A, Kisslo J, Weyman A. Recommendations regarding quantitation in M-mode echocardiography: results of a survey of echocardiographic measurements. *Circulation* 1978;**58**:1072-1083.
74. Teichholz LE, Kreulen T, Herman MV, Gorlin R. Problems in echocardiographic volume determinations: echocardiographic-angiographic correlations in the presence of absence of asynergy. *Am J Cardiol* 1976;**37**:7-11.
75. Patel K, Tiwari N, Aronow WS, Spevack D. Can the echocardiographic LV mass equation reliably demonstrate stable LV mass following acute change in LV load? *Ann Transl Med* 2019;**7**:3.
76. Pawlush DG, Moore RL, Musch TI, Davidson WR, Jr. Echocardiographic evaluation of size, function, and mass of normal and hypertrophied rat ventricles. *J Appl Physiol (1985)* 1993;**74**:2598-2605.
77. Inoko M, Kihara Y, Morii I, Fujiwara H, Sasayama S. Transition from compensatory hypertrophy to dilated, failing left ventricles in Dahl salt-sensitive rats. *Am J Physiol* 1994;**267**:H2471-2482.
78. Youn HJ, Rokosh G, Lester SJ, Simpson P, Schiller NB, Foster E. Two-dimensional echocardiography with a 15-MHz transducer is a promising alternative for in vivo measurement of left ventricular mass in mice. *J Am Soc Echocardiogr* 1999;**12**:70-75.
79. Cheung MC, Spalding PB, Gutierrez JC, Balkan W, Namias N, Koniaris LG, Zimmers TA. Body surface area prediction in normal, hypermuscular, and obese mice. *J Surg Res* 2009;**153**:326-331.
80. Gouma E, Simos Y, Verginadis I, Lykoudis E, Evangelou A, Karkabounas S. A simple procedure for estimation of total body surface area and determination of a new value of Meeh's constant in rats. *Lab Anim* 2012;**46**:40-45.
81. Ballo H, Tarkia M, Haavisto M, Stark C, Strandberg M, Vahasilta T, Saunavaara V, Tolvanen T, Teras M, Hynninen VV, Savunen T, Roivainen A, Knuuti J, Saraste A. Accuracy of echocardiographic area-length method in chronic myocardial infarction: comparison with cardiac CT in pigs. *Cardiovasc Ultrasound* 2017;**15**:1.
82. Wyatt HL, Heng MK, Meerbaum S, Gueret P, Hestenes J, Dula E, Corday E. Cross-sectional echocardiography. II. Analysis of mathematic models for quantifying volume of the formalin-fixed left ventricle. *Circulation* 1980;**61**:1119-1125.

83. Benavides-Vallve C, Corbacho D, Iglesias-Garcia O, Pelacho B, Albiasu E, Castano S, Munoz-Barrutia A, Prosper F, Ortiz-de-Solorzano C. New strategies for echocardiographic evaluation of left ventricular function in a mouse model of long-term myocardial infarction. *PLoS One* 2012;**7**:e41691.
84. Kanno S, Lerner DL, Schuessler RB, Betsuyaku T, Yamada KA, Saffitz JE, Kovacs A. Echocardiographic evaluation of ventricular remodeling in a mouse model of myocardial infarction. *J Am Soc Echocardiogr* 2002;**15**:601-609.
85. Quinones MA, Otto CM, Stoddard M, Waggoner A, Zoghbi WA, Doppler Quantification Task Force of the N, Standards Committee of the American Society of E. Recommendations for quantification of Doppler echocardiography: a report from the Doppler Quantification Task Force of the Nomenclature and Standards Committee of the American Society of Echocardiography. *J Am Soc Echocardiogr* 2002;**15**:167-184.
86. Tournoux F, Petersen B, Thibault H, Zou L, Raher MJ, Kurtz B, Halpern EF, Chaput M, Chao W, Picard MH, Scherrer-Crosbie M. Validation of noninvasive measurements of cardiac output in mice using echocardiography. *J Am Soc Echocardiogr* 2011;**24**:465-470.
87. Pfeffer MA, Shah AM, Borlaug BA. Heart Failure With Preserved Ejection Fraction In Perspective. *Circ Res* 2019;**124**:1598-1617.
88. Ponikowski P, Voors AA, Anker SD, Bueno H, Cleland JG, Coats AJ, Falk V, Gonzalez-Juanatey JR, Harjola VP, Jankowska EA, Jessup M, Linde C, Nihoyannopoulos P, Parissis JT, Pieske B, Riley JP, Rosano GM, Ruilope LM, Ruschitzka F, Rutten FH, van der Meer P, Authors/Task Force M, Document R. 2016 ESC Guidelines for the diagnosis and treatment of acute and chronic heart failure: The Task Force for the diagnosis and treatment of acute and chronic heart failure of the European Society of Cardiology (ESC). Developed with the special contribution of the Heart Failure Association (HFA) of the ESC. *Eur J Heart Fail* 2016;**18**:891-975.
89. Senni M, Paulus WJ, Gavazzi A, Fraser AG, Diez J, Solomon SD, Smiseth OA, Guazzi M, Lam CS, Maggioni AP, Tschope C, Metra M, Hummel SL, Edelmann F, Ambrosio G, Stewart Coats AJ, Filippatos GS, Gheorghiade M, Anker SD, Levy D, Pfeffer MA, Stough WG, Pieske BM. New strategies for heart failure with preserved ejection fraction: the importance of targeted therapies for heart failure phenotypes. *Eur Heart J* 2014;**35**:2797-2815.
90. Guazzi M, Dixon D, Labate V, Beussink-Nelson L, Bandera F, Cuttica MJ, Shah SJ. RV Contractile Function and its Coupling to Pulmonary Circulation in Heart Failure With Preserved Ejection Fraction: Stratification of Clinical Phenotypes and Outcomes. *JACC Cardiovasc Imaging* 2017;**10**:1211-1221.
91. Mohammed SF, Hussain I, AbouEzzeddine OF, Takahama H, Kwon SH, Forfia P, Roger VL, Redfield MM. Right ventricular function in heart failure with preserved ejection fraction: a community-based study. *Circulation* 2014;**130**:2310-2320.
92. Hamdani N, Franssen C, Lourenco A, Falcao-Pires I, Fontoura D, Leite S, Plettig L, Lopez B, Ottenheijm CA, Becher PM, Gonzalez A, Tschope C, Diez J, Linke WA, Leite-Moreira AF, Paulus WJ. Myocardial titin hypophosphorylation importantly contributes to heart failure with preserved ejection fraction in a rat metabolic risk model. *Circ Heart Fail* 2013;**6**:1239-1249.
93. Nguyen TD, Shingu Y, Schwarzer M, Schrepper A, Doenst T. The E-wave deceleration rate E/DT outperforms the tissue Doppler-derived index E/e' in characterizing lung remodeling in heart failure with preserved ejection fraction. *PLoS One* 2013;**8**:e82077.
94. Schnelle M, Catibog N, Zhang M, Nabeebaccus AA, Anderson G, Richards DA, Sawyer G, Zhang X, Toischer K, Hasenfuss G, Monaghan MJ, Shah AM. Echocardiographic evaluation of diastolic function in mouse models of heart disease. *J Mol Cell Cardiol* 2018;**114**:20-28.
95. Miranda-Silva D, Goncalves-Rodrigues P, Almeida-Coelho J, Hamdani N, Lima T, Conceicao G, Sousa-Mendes C, Claudia M, Gonzalez A, Diez J, Linke WA, Leite-Moreira A, Falcao-Pires I. Characterization of biventricular alterations in myocardial (reverse) remodelling in aortic banding-induced chronic pressure overload. *Sci Rep* 2019;**9**:2956.
96. Lourenco AP, Leite-Moreira AF, Balligand JL, Bauersachs J, Dawson D, de Boer RA, de Windt LJ, Falcao-Pires I, Fontes-Carvalho R, Franz S, Giacca M, Hilfiker-Kleiner D, Hirsch E, Maack C, Mayr M, Pieske B, Thum T, Tocchetti CG, Brutsaert DL, Heymans S. An integrative translational approach to study heart failure with preserved ejection fraction: a position paper from the Working Group on Myocardial Function of the European Society of Cardiology. *Eur J Heart Fail* 2018;**20**:216-227.
97. Leite S, Oliveira-Pinto J, Tavares-Silva M, Abdellatif M, Fontoura D, Falcao-Pires I, Leite-Moreira AF, Lourenco AP. Echocardiography and invasive hemodynamics during stress testing for diagnosis of heart failure with preserved ejection fraction: an experimental study. *Am J Physiol Heart Circ Physiol* 2015;**308**:H1556-1563.
98. Fraysse B, Weinberger F, Bardswell SC, Cuello F, Vignier N, Geertz B, Starbatty J, Kramer E, Coirault C, Eschenhagen T, Kentish JC, Avkiran M, Carrier L. Increased myofilament Ca2+ sensitivity and diastolic dysfunction as early consequences of Mybpc3 mutation in heterozygous knock-in mice. *J Mol Cell Cardiol* 2012;**52**:1299-1307.
99. Szardien S, Nef HM, Voss S, Troidl C, Liebetrau C, Hoffmann J, Rauch M, Mayer K, Kimmich K, Rolf A, Rixe J, Troidl K, Kojonazarov B, Schermuly RT, Kostin S, Elsasser A, Hamm CW, Mollmann H. Regression of cardiac hypertrophy by granulocyte colony-stimulating factor-stimulated interleukin-1beta synthesis. *Eur Heart J* 2012;**33**:595-605.

100. Zhang L, Jaswal JS, Ussher JR, Sankaralingam S, Wagg C, Zaugg M, Lopaschuk GD. Cardiac insulin-resistance and decreased mitochondrial energy production precede the development of systolic heart failure after pressure-overload hypertrophy. *Circ Heart Fail* 2013;**6**:1039-1048.
101. Pritchett AM, Mahoney DW, Jacobsen SJ, Rodeheffer RJ, Karon BL, Redfield MM. Diastolic dysfunction and left atrial volume: a population-based study. *J Am Coll Cardiol* 2005;**45**:87-92.
102. Nagueh SF, Smiseth OA, Appleton CP, Byrd BF, 3rd, Dokainish H, Edvardsen T, Flachskampf FA, Gillebert TC, Klein AL, Lancellotti P, Marino P, Oh JK, Alexandru Popescu B, Waggoner AD, Houston T, Oslo N, Phoenix A, Nashville T, Hamilton OC, Uppsala S, Ghent, Liege B, Cleveland O, Novara I, Rochester M, Bucharest R, St. Louis M. Recommendations for the Evaluation of Left Ventricular Diastolic Function by Echocardiography: An Update from the American Society of Echocardiography and the European Association of Cardiovascular Imaging. *Eur Heart J Cardiovasc Imaging* 2016;**17**:1321-1360.
103. Oki T, Tabata T, Yamada H, Wakatsuki T, Shinohara H, Nishikado A, Iuchi A, Fukuda N, Ito S. Clinical application of pulsed Doppler tissue imaging for assessing abnormal left ventricular relaxation. *Am J Cardiol* 1997;**79**:921-928.
104. Huis In 't Veld AE, de Man FS, van Rossum AC, Handoko ML. How to diagnose heart failure with preserved ejection fraction: the value of invasive stress testing. *Neth Heart J* 2016;**24**:244-251.
105. Paulus WJ, Tschope C, Sanderson JE, Rusconi C, Flachskampf FA, Rademakers FE, Marino P, Smiseth OA, De Keulenaer G, Leite-Moreira AF, Borbely A, Edes I, Handoko ML, Heymans S, Pezzali N, Pieske B, Dickstein K, Fraser AG, Brutsaert DL. How to diagnose diastolic heart failure: a consensus statement on the diagnosis of heart failure with normal left ventricular ejection fraction by the Heart Failure and Echocardiography Associations of the European Society of Cardiology. *Eur Heart J* 2007;**28**:2539-2550.
106. Park JH, Marwick TH. Use and Limitations of E/e' to Assess Left Ventricular Filling Pressure by Echocardiography. *J Cardiovasc Ultrasound* 2011;**19**:169-173.
107. Schaefer A, Meyer GP, Hilfiker-Kleiner D, Brand B, Drexler H, Klein G. Evaluation of Tissue Doppler Tei index for global left ventricular function in mice after myocardial infarction: comparison with Pulsed Doppler Tei index. *Eur J Echocardiogr* 2005;**6**:367-375.
108. Helbing WA, Bosch HG, Maliepaard C, Rebergen SA, van der Geest RJ, Hansen B, Ottenkamp J, Reiber JH, de Roos A. Comparison of echocardiographic methods with magnetic resonance imaging for assessment of right ventricular function in children. *Am J Cardiol* 1995;**76**:589-594.
109. Evangelista A, Flachskampf F, Lancellotti P, Badano L, Aguilar R, Monaghan M, Zamorano J, Nihoyannopoulos P, European Association of E. European Association of Echocardiography recommendations for standardization of performance, digital storage and reporting of echocardiographic studies. *Eur J Echocardiogr* 2008;**9**:438-448.
110. Moreth K, Fischer R, Fuchs H, Gailus-Durner V, Wurst W, Katus HA, Bekeredjian R, Hrabe de Angelis M. High-throughput phenotypic assessment of cardiac physiology in four commonly used inbred mouse strains. *J Comp Physiol B* 2014;**184**:763-775.
111. Vinhas M, Araujo AC, Ribeiro S, Rosario LB, Belo JA. Transthoracic echocardiography reference values in juvenile and adult 129/Sv mice. *Cardiovasc Ultrasound* 2013;**11**:12.
112. Baumann PQ, Sobel BE, Tarikuz Zaman AK, Schneider DJ. Gender-dependent differences in echocardiographic characteristics of murine hearts. *Echocardiography* 2008;**25**:739-748.

Figure legends

Figure 1: Recommendations for preparing the animal and finalizing the echocardiographic exam. Do not forget to register: 1) mouse/rat strain, sex, age and weight; 2) equipment used (model and probe) and 3) anesthesia type and dose.

Figure 2: Standard echocardiographic views. For each projection, we describe the parameters that should be measured as well as its derived parameters. A, late diastolic transmitral flow velocity; AV, aortic valve; CO, cardiac output; DT, deceleration time; E, early diastolic transmitral flow velocity; e’, peak early-diastolic annular velocity; EF, ejection fraction; FS, fractional shortening; HR, heart rate; IVRT, isovolumic relaxation time; IVSd, interventricular septum thickness in diastole; IVSs, interventricular septum thickness in systole; LAA, left atrial area; LV, left ventricle; LVEDV, left ventricular end-diastolic volume; LVEDA, left ventricular end-diastolic area; LVESA, left ventricular end-systolic area; LVESV, left ventricular end-systolic volume; LVIDd, left ventricle internal diameter in diastole; LVIDs, left ventricle internal diameter in systole; LV mass, left ventricle mass; LVAWd, left ventricular anterior wall thickness in diastole; LVAWs, left ventricular anterior wall thickness in systole; LVPWd, left ventricular posterior wall thickness in diastole; LVPWs, left ventricular posterior wall thickness in systole; MPI, myocardial performance (Tei) index; RA, right atria; RV, right ventricle; RWT, relative wall thickness; s’, peak systolic annular velocity; SV, stroke volume; VTI, velocity time integral; PW, pulsed wave.

Figure 3: Common pitfalls when assessing systolic and diastolic function in HFrEF and HFpEF animal models. LV, left ventricle; PA, pulmonary artery; pv, pulmonary valve; pm, papillary muscle; IVS, interventricular septum; RV, right ventricle; LA, left atrium; mv, mitral valve; MV A, late diastolic transmitral flow velocity; a’, late early-diastolic annular velocity; MV E, early diastolic transmitral flow velocity; e’, peak early-diastolic annular velocity; IVRT, isovolumic relaxation time; IVCT, isovolumetric contraction time; AET, aortic ejection time; HR, heart rate; bpm, beats-per-minute. Echocardiographic exams were performed using a Vevo 3100 Imaging System (VisualSonics).

Figure 4: Longitudinal and short-axis views in healthy and pathological conditions. All the acquisitions were made at end-diastole as determined with ECG and respiratory tracing (movies corresponding to each image, showing physiological parameters, are included as Supplementary material, **Videos 10-21**). Echocardiographic exams were performed using a Vevo 3100 Imaging System (VisualSonics).

Legend to the graphical abstract

Graphical abstract – workflow of an echocardiographic exam. For each projection, we describe the parameters that should be measured as well as their derived parameters. **A**, late diastolic transmitral flow velocity; **AV**, aortic valve; **CO**, cardiac output; **DT**, deceleration time; **E,** early diastolic transmitral flow velocity; **e'**, peak early-diastolic annular velocity; **EF**, ejection fraction; **FS**, fractional shortening; **HR**, heart rate; **IVRT**, isovolumic relaxation time; **IVSd**, interventricular septum thickness in diastole; **IVSs**, interventricular septum thickness in systole; **LAA**, left atrial area; **LV**, left ventricle; **LVEDV**, left ventricular end-diastolic volume; **LVEDA**, left ventricular end-diastolic area; **LVESA**, left ventricular end-systolic area; **LVESV**, left ventricular end-systolic volume; **LVIDd**, left ventricle internal diameter in diastole; **LVIDs**, left ventricle internal diameter in systole; **LV mass**, left ventricle mass; **LVAWd**, left ventricular anterior wall thickness in diastole; **LVAWs**, left ventricular anterior wall thickness in systole**; LVPWd**, left ventricular posterior wall thickness in diastole; **LVPWs**, left ventricular posterior wall thickness in systole; **RV**, right ventricle; **s',** peak systolic annular velocity; **SV**, stroke volume; **VTI**, velocity time integral; **PW**, pulsed wave.

Table 1

Table 1. Echocardiographic parameters and indexes of LV function in control/healthy Wistar Han rats comparing two types of anesthesia. Acquisitions were made with a GE Vivid 7 system or a Siemens Sequoia using a 12MHz transducer, in over 100 animals. Values are presented as mean ± SD. A, late diastolic transmitral flow velocities; BW, body weight; CO, cardiac output; E, early diastolic transmitral flow velocities; e', peak early-diastolic annular velocity; EF, ejection fraction; FS, fractional shortening; HR, heart rate; IVRT, isovolumic relaxation time; IVSd, interventricular septum thickness in diastole; IVSs, interventricular septum thickness in systole; LAA, left atrial area; LVEDV, left ventricular end-diastolic volume; LVESV, left ventricular end-systolic volume; LVIDd, left ventricle internal diameter in diastole; LVIDs, left ventricle internal diameter in systole; LV mass, left ventricle mass; LVPWd, left ventricular posterior wall thickness in diastole; LVPWs, left ventricular posterior wall thickness in systole; MPI, myocardial performance (Tei) index; s', peak systolic annular velocity; SV, stroke volume.

[redacted]	[redacted]	[redacted]
BW (g)	382 ± 26	364 ± 44
HR (bpm)	383 ± 33	340 ± 10
LVmass (mg)	645 ± 93	745 ± 30
LVPWd (mm)	1.44 ± 0.17	1.60 ± 0.23
LVPWs (mm)	2.23 ± 0.40	2.56 ± 0.51
LVIDs (mm)	4.03 ± 0.40	3.53 ± 0.67
LVIDd (mm)	6.88 ± 0.44	6.73 ± 0.43
IVSd (mm)	1.52 ± 0.20	1.58 ±0.05
IVSs (mm)	2.51 ± 0.42	2.63 ±0.43
LVESV (µm)	72.3 ± 17.1	49.9 ±19
LVEDV (µm)	247 ± 35	232 ± 34
EF (%)	70.6 ± 5.9	79.9 ± 6.3
FS (%)	41.4 ± 5.0	47.8 ± 7.7
SV (µL)	175 ± 31	182 ± 24
CO (mL/min)	68.3 ± 11.2	62.3 ± 11.6
s' (mm/s)	53.4 ± 9.7	58.0 ± 5.1
E (mm/s)	774 ± 171	741 ± 155
A (mm/s)	540 ± 136	454 ± 73
E/A	1.44 ± 0.22	1.73 ± 0.40
E slope (mm/s)	19.7 ± 4.5	n.a.
IVRT (ms)	17.8 ± 4.3	16.4 ± 6.1
MPI (Tei)	0.50 ± 0.14	0.35 ± 0.05
e' (mm/s)	58.0 ± 14.8	47.4 ± 11.6
E/e'	13.4 ± 2.2	16.7 ± 5.5
LAA (cm^2)	2.94 ± 0.41	3.36 ± 0.30

Table 2

Table 2. Echocardiographic parameters and indexes of LV function in control/healthy C57BL/6 mice. All acquisitions were made with mice under halogenated gases anesthesia (isoflurane or sevoflurane). The results presented in this table derive from over 300 exams performed across 10 different laboratories and are shown in separate columns for mice keeping HR in its physiological range (> 450 bpm) or depressed by anesthesia (< 450 bpm). Echocardiographic exams were made with a Vevo 770, 2100 or 3100 Imaging System (VisualSonics) or a Aloka SSD 4000. Values are presented as mean ±S D. BW, body weight; CO, cardiac output; EF, ejection fraction; FS, fractional shortening; HR, heart rate; IVSd, interventricular septum thickness in diastole; IVSs, interventricular septum thickness in systole; LAA, left atrial area; LVEDV, left ventricular end-diastolic volume; LVESV, left ventricular end-systolic volume; LVIDd, left ventricle internal diameter in diastole; LVIDs, left ventricle internal diameter in systole; LV mass, left ventricle mass; LVPWd, left ventricular posterior wall thickness in diastole; LVPWs, left ventricular posterior wall thickness in systole; SV, stroke volume. All values are presented as mean ± standard deviation.

BW (g)	25.7±3.6	24.6 ± 2.6
HR (bpm)	535 ± 75	418 ± 19
LV mass (mg)	96 ± 18	99 ± 17
LVPWd (mm)	0.79 ± 0.22	0.58 ± 0.18
LVPWs (mm)	1.12 ± 0.33	0.84 ± 0.12
LVIDs (mm)	2.20 ± 0.50	2.69 ± 0.39
LVIDd (mm)	3.69 ± 0.41	3.95 ± 0.28
IVSd (mm)	0.71 ± 0.15	0.93 ± 0.12
IVSs (mm)	0.97 ±0.19	1.14 ± 0.14
LVESV (µL)	19.35 ± 11.3	29.09 ± 10.4
LVEDV (µL)	57.7 ± 16.5	66.3 ± 11.6
EF (%)	71 ± 11	58 ± 11
FS (%)	43 ± 9	31 ± 8
SV (µL)	35.1 ± 8.5	31.0 ± 6.0
CO (mL/min)	17.7 ± 3.8	14.76
s' (mm/s)	46 ± 7	30 ± 17
E (mm/s)	718 ± 109	648 ± 111
A (mm/s)	455 ± 105	427 ± 95
E/A	1.52 ± 0.4	1.42 ± 0.26
IVRT (ms)	17.3 ± 4.2	17.1 ± 2.5
MPI (Tei)	0.66 ± 0.17	n.a.
e' (mm/s)	43.2 ± 10.9	26.5 ± 1.2
E/e'	15.2 ± 6.7	24.5 ± 14.3
LAA (mm^2)	2.6 ± 0.4	3.5± 2.3

Table 3. Echocardiographic views and parameters that should be specifically recorded to characterize cardiac function when working with distinct animal models. **A,** late diastolic transmitral flow velocities; **BW**, body weight; **CO**, cardiac output; **E,** early diastolic transmitral flow velocities; **e'**, peak early-diastolic annular velocity; **EF,** ejection fraction; **FS,** fractional shortening; **HR**, heart rate; **IVRT,** isovolumic relaxation time; **IVSd**, interventricular septum thickness in diastole; **IVSs**, interventricular septum thickness in systole; **LAA**, left atrial area; **LVEDV**, left ventricular end-diastolic volume; **LVESV,** left ventricular end-systolic volume; **LVIDd**, left ventricle internal diameter in diastole; **LVIDs**, left ventricle internal diameter in systole; **LV mass,** left ventricle mass; **LVPWd**, left ventricular posterior wall thickness in diastole; **LVPWs**, left ventricular posterior wall thickness in systole; **MPI,** myocardial performance (Tei) index; **RWT**, relative wall thickness; **s'**, peak systolic annular velocity; **SV**, stroke volume.

Chronic pressure overload	Two-dimensional B-mode and M-mode, parasternal long and/or short-axis view	Record diastolic and systolic LV wall thickness and chamber dimensions to calculate: - LVESV = (7 / (2.4 + LVIDs)) x LVIDs^3 - LVEDV = (7 / (2.4 + LVIDd)) x LVIDd^3 - FS (%) = (LVIDd - LVIDs) / LVIDd x 100 - EF (%) = (LVEDV - LVESV) / LVEDV x 100 - LV mass (mg) = 1.04 [(LVIDd + LVAWd + LVPWd)^3 - LVIDd^3] x 0.8 + 0.6 - Stroke volume, SV (µl) = (LVEDV – LVESV) - Cardiac output (µl/min): CO = SV x HR - Relative wall thickness: RWT = (LVPWd + LVIVSd) / (LVIDd)
	Two-dimensional PW doppler echocardiography, supra-sternal or neck position	Record the pressure gradient across the constricted portion of ascending aorta and/or the right/left carotid velocity flow ratio (expected to be 5-10)
	Pulsed wave Doppler mode and Tissue Doppler mode, apical four- or five-chamber views	Record diastolic parameters: - Early and late mitral filling velocities (E and A wave) - E wave deceleration time (DT) - Early diastolic mitral annular tissue velocity (e') - Isovolumic relaxation time (IVRT) - Ejection time (ET)
	Two-dimensional B-mode, apical four-chamber view	Measure Left atrium area (LAA)
Myocardial infarction	Two-dimensional B-mode and M-mode, parasternal long-axis and short-axis views	Record diastolic and systolic LV wall thickness and chamber size and use the Simpson's method to calculate: - LV area at the level of mitral valve (A1, as in Figure 4, panels a) in systole and diastole - LV area at the level of the papillary muscles (A2, as in Figure 4, panels b) in systole and diastole - LV area at the level of the apex (A3, as in Figure 4, panels c) in systole and diastole - The maximum length of the ventricle in parasternal long-axis, in systole (LVESL) and diastole (LVEDL) - LVEDV = (A1+A2) x (LVEDL/3) + (A3/2) x (LVEDL/3) + (π/6) x (LVEDL/3)^3 - LVESV = (A1+A2) x (LVESL/3) + (A3/2) x (LVESL/3) + (π/6) x (LVESL/3)^3 - EF (%) = (LVEDV-LVESV) / LVEDV x 100 - Aortic annulus diameter
	Pulsed wave Doppler and Tissue Doppler mode, apical four- or five-chamber view at the medial mitral annulus	Record systolic parameters: - Isovolumetric contraction time (IVCT) - Ejection time (ET) - Myocardial performance index (MPI/Tei) = (IVCT + IVRT) / ET - LV systolic myocardial velocity (s') at the level of the septal mitral annulus Record and calculate aortic parameters: - Aortic annulus velocity (VTI) - SV = VTI x aortic annulus diameter
Diastolic dysfunction and HFpEF	Two-dimensional B-mode and M-mode, parasternal long and/or short-axis view	Record diastolic and systolic LV wall thickness and chamber dimensions to calculate: - LVESV = (7 / (2.4 + LVIDs)) x LVIDs^3 - LVEDV = (7 / (2.4 + LVIDd)) x LVIDd^3 - FS (%) = (LVIDd - LVIDs) / LVIDd x 100 - EF (%) = (LVEDV - LVESV) / LVEDV x 100 - LV mass (mg) = 1.04 [(LVIDd + LVAWd + LVPWd)^3 - LVIDd^3] x 0.8 + 0.6 - Stroke volume, SV (µl) = (LVEDV – LVESV) - Cardiac output (µl/min): CO = SV x HR - Relative wall thickness: RWT = (LVPWd + LVIVSd) / (LVIDd)
	Pulsed wave Doppler or Tissue Doppler mode, apical four-chamber view at the medial mitral annulus	Record diastolic parameters: - Early and late mitral filling velocities (E and A wave) - E wave deceleration time - Isovolumic relaxation time (IVRT) - Peak mitral annular velocity (E´) during early filling at septal or lateral corner of the mitral annulus. Record systolic parameters: - Ejection time (ET) - LV index of myocardial performance = (IVCT+IVRT)/ET - Peak systolic tissue velocity (s') at the medial mitral annulus

	Two-dimensional B-mode, apical four-chamber view	Measure Left atrium area (LAA)

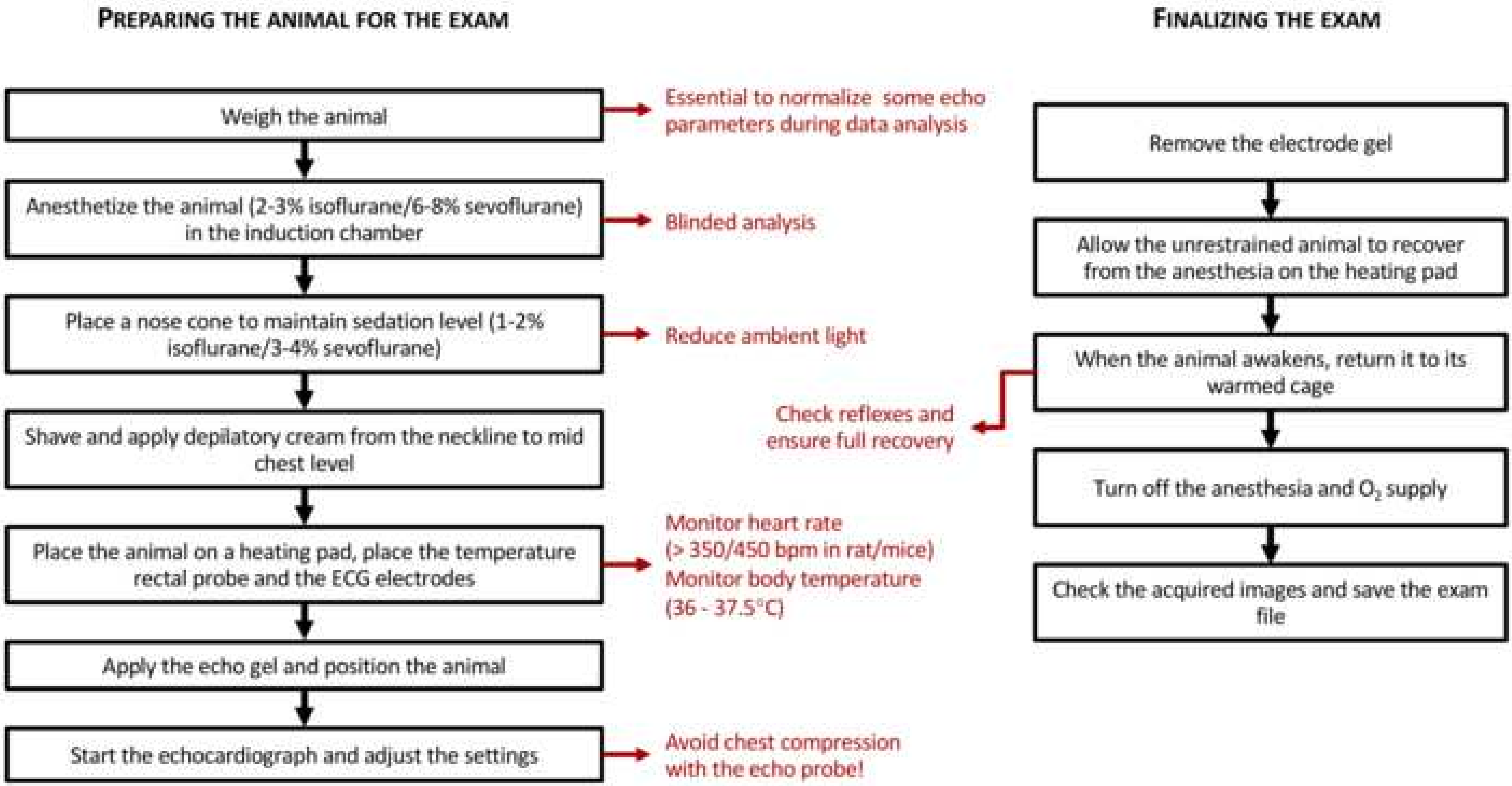

PREPARING THE ANIMAL FOR THE EXAM

Weigh the animal

Anesthetize the animal (2-3% isoflurane/6-8% sevoflurane) in the induction chamber

Place a nose cone to maintain sedation level (1-2% isoflurane/3-4% sevoflurane)

Shave and apply depilatory cream from the neckline to mid chest level

Place the animal on a heating pad, place the temperature rectal probe and the ECG electrodes

Apply the echo gel and position the animal

Start the echocardiograph and adjust the settings

Essential to normalize some echo parameters during data analysis

Blinded analysis

Reduce ambient light

Monitor heart rate (> 350/450 bpm in rat/mice)

Monitor body temperature (36 - 37.5°C)

Avoid chest compression with the echo probe!

FINALIZING THE EXAM

Remove the electrode gel

Allow the unrestrained animal to recover from the anesthesia on the heating pad

When the animal awakens, return it to its warmed cage

Check reflexes and ensure full recovery

Turn off the anesthesia and O_2 supply

Check the acquired images and save the exam file

Figure 1

Figure 2

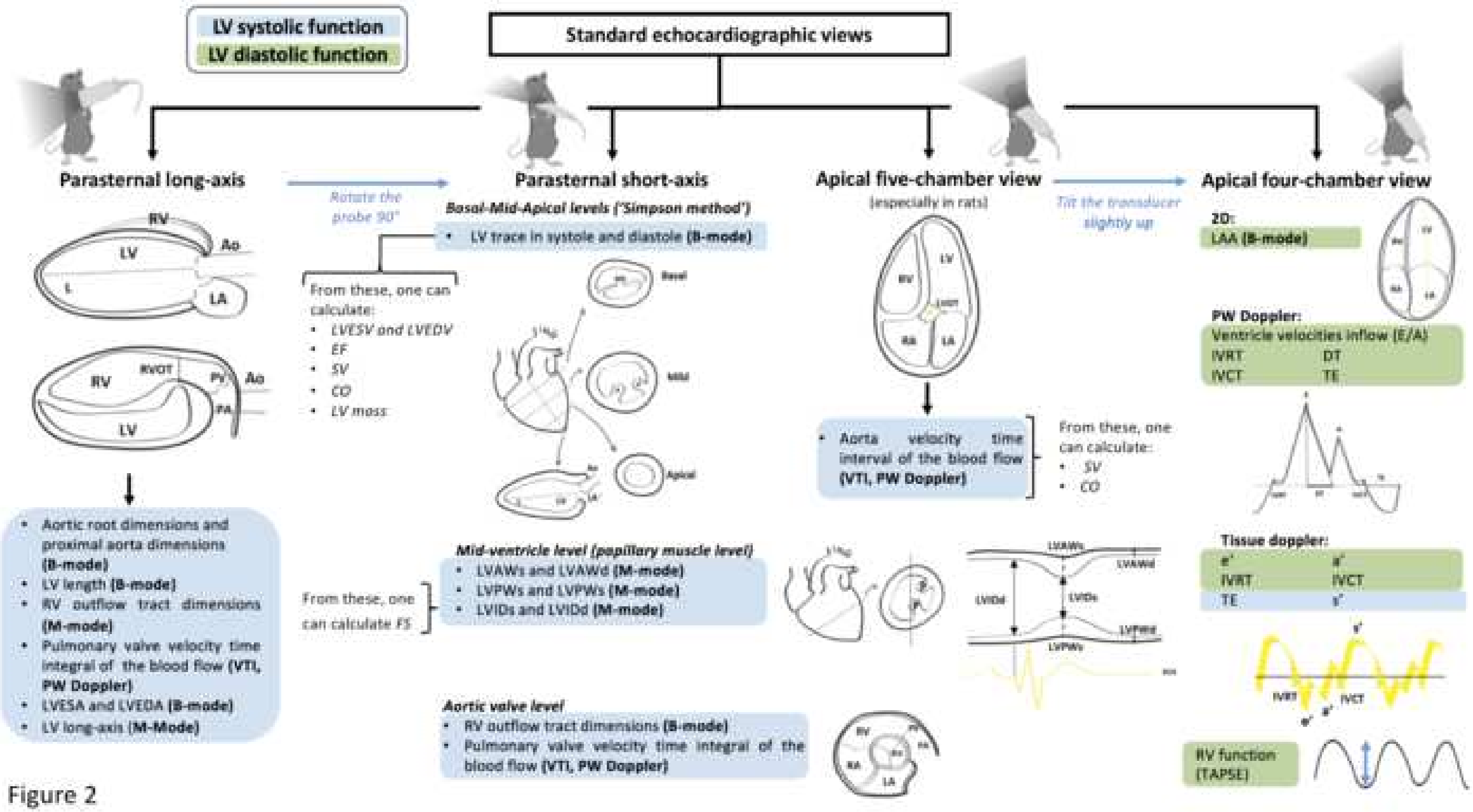

Figure 2

Figure 3

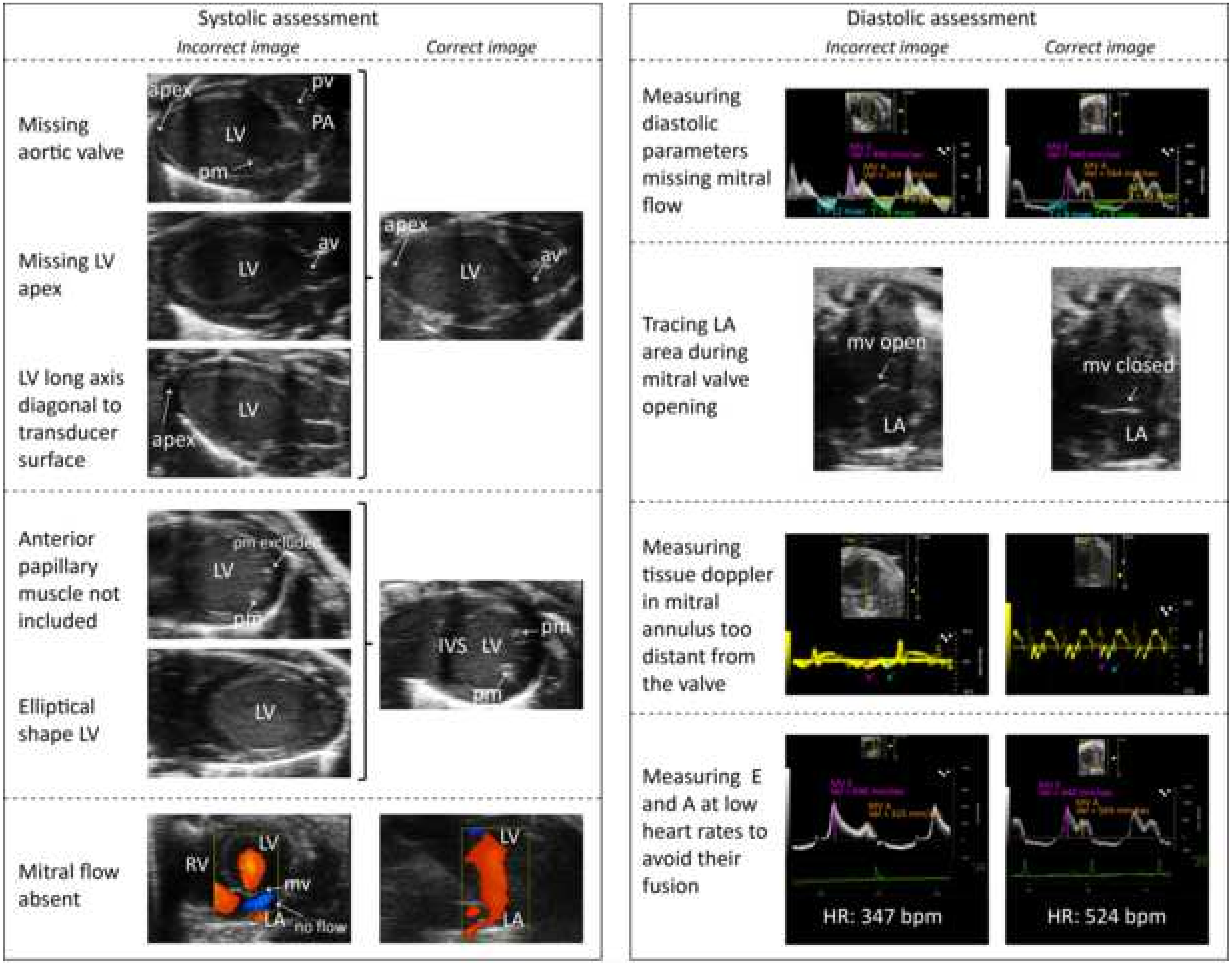

Other common pitfalls are: 1) too much light in the room; 2) HR below 350 or 450 bpm in rats and mice, respectively; 3) animal hypotermia due to cold room temperature or heating pad turned off. Representative images were acquired in mice.

Figure 3

Figure 4

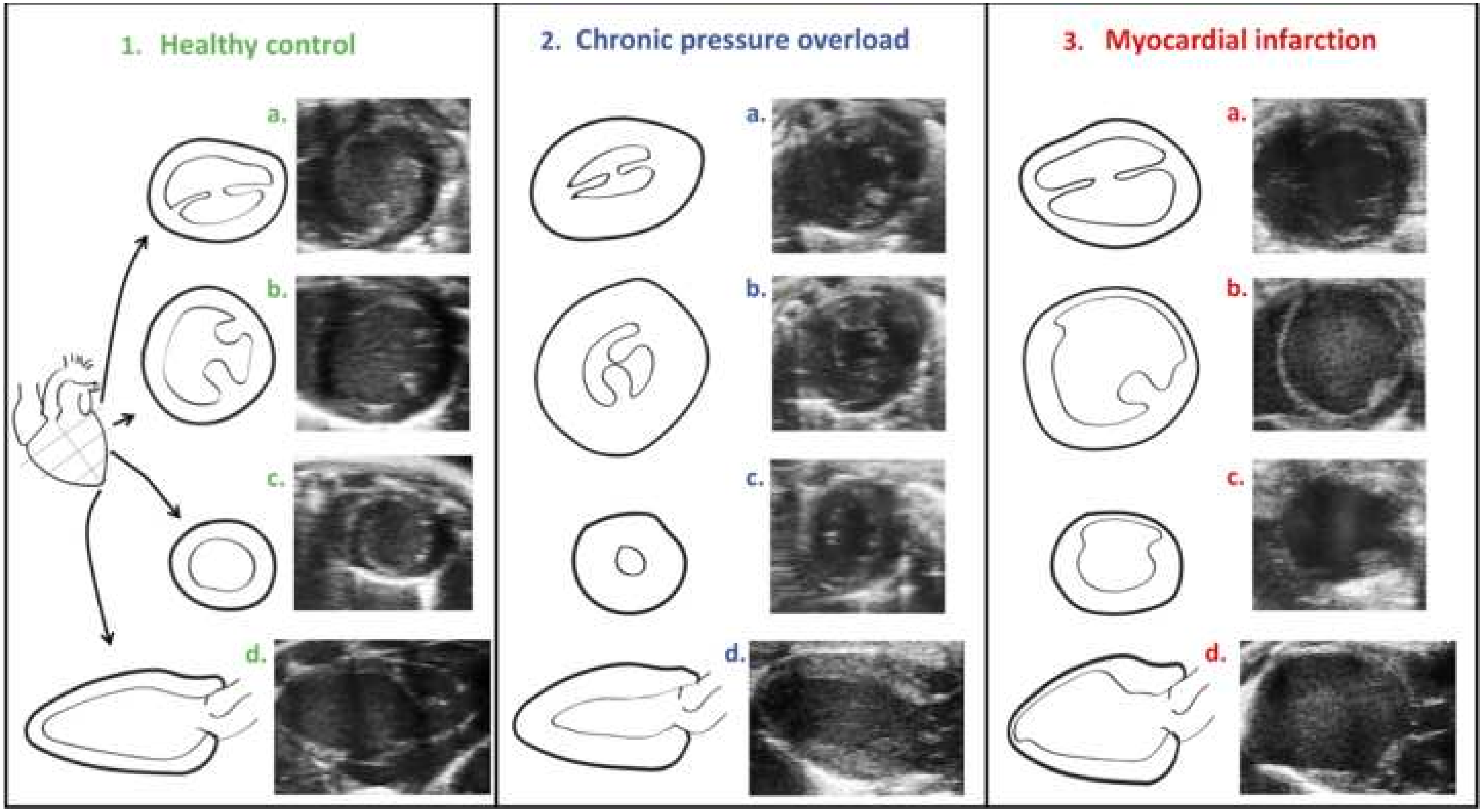
1. Healthy control
a.
b.
c.
d.
2. Chronic pressure overload
a.
b.
c.
d.
3. Myocardial infarction
a.
b.
c.
d.

Graphical Abstract

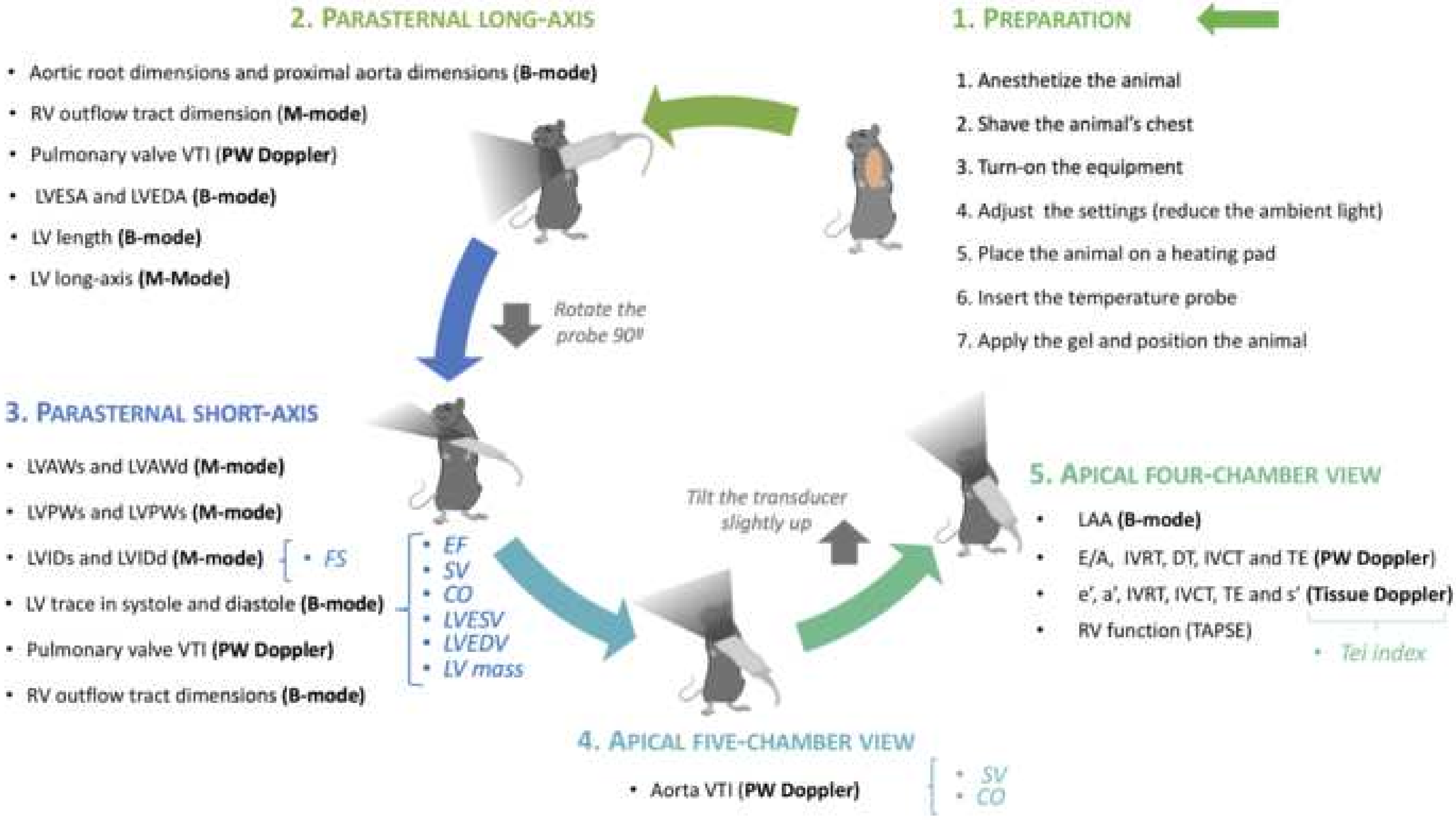

1. PREPARATION

1. Anesthetize the animal
2. Shave the animal's chest
3. Turn-on the equipment
4. Adjust the settings (reduce the ambient light)
5. Place the animal on a heating pad
6. Insert the temperature probe
7. Apply the gel and position the animal

2. PARASTERNAL LONG-AXIS

- Aortic root dimensions and proximal aorta dimensions (**B-mode**)
- RV outflow tract dimension (**M-mode**)
- Pulmonary valve VTI (**PW Doppler**)
- LVESA and LVEDA (**B-mode**)
- LV length (**B-mode**)
- LV long-axis (**M-Mode**)

Rotate the probe 90°

3. PARASTERNAL SHORT-AXIS

- LVAWs and LVAWd (**M-mode**)
- LVPWs and LVPWs (**M-mode**)
- LVIDs and LVIDd (**M-mode**) – *FS*
- LV trace in systole and diastole (**B-mode**) – *EF*, *SV*, *CO*, *LVESV*, *LVEDV*, *LV mass*
- Pulmonary valve VTI (**PW Doppler**)
- RV outflow tract dimensions (**B-mode**)

Tilt the transducer slightly up

4. APICAL FIVE-CHAMBER VIEW

- Aorta VTI (**PW Doppler**) – *SV*, *CO*

5. APICAL FOUR-CHAMBER VIEW

- LAA (**B-mode**)
- E/A, IVRT, DT, IVCT and TE (**PW Doppler**)
- e', a', IVRT, IVCT, TE and s' (**Tissue Doppler**) – *Tei index*
- RV function (TAPSE)